Pergamon

Int. J. Solids Structures Vol. 33, No. 7, pp. 931–966, 1996
Copyright © 1995 Elsevier Science Ltd
Printed in Great Britain. All rights reserved
0020-7683/96 $15.00 + .00

0020-7683(95)00084-4

THERMOELASTIC THEORY FOR THE RESPONSE OF MATERIALS FUNCTIONALLY GRADED IN TWO DIRECTIONS

JACOB ABOUDI†, MAREK-JERZY PINDERA
Civil Engineering & Applied Mechanics Department, University of Virginia, Charlottesville, VA 22903, U.S.A.

and

STEVEN M. ARNOLD
Structural Fatigue Branch, NASA-Lewis Research Center, Cleveland, OH 44135, U.S.A.

(*Received 2 November* 1994; *in revised form 28 March* 1995)

Abstract—A recently developed micromechanical theory for the thermoelastic response of functionally graded composites with nonuniform fiber spacing in the through-thickness direction is further extended to enable analysis of material architectures characterized by arbitrarily nonuniform fiber spacing in two directions. In contrast to currently employed micromechanical approaches applied to functionally graded materials, which decouple the local and global effects by assuming the existence of a representative volume element at every point within the composite, the new theory explicitly couples the local and global effects. The analytical development is based on volumetric averaging of the various field quantities, together with imposition of boundary and interfacial conditions in an average sense. Results are presented that illustrate the capability of the derived theory to capture local stress gradients at the free edge of a laminated composite plate due to the application of a uniform temperature change. It is further shown that it is possible to reduce the magnitude of these stress concentrations by a proper management of the microstructure of the composite plies near the free edge. Thus by an appropriate tailoring of the microstructure it is possible to reduce or prevent the likelihood of delamination at free edges of standard composite laminates.

NOMENCLATURE

p, q, r	indices used to identify the cell (p, q, r)
N_q, N_r	number of cells in the x_2 and x_3 directions, respectively
α, β, γ	indices used to identify the subcell $(\alpha\beta\gamma)$
$d_\alpha, h_\beta^{(q)}, l_\gamma^{(r)}$	dimensions of the subcell $(\alpha\beta\gamma)$ in the (p, q, r)th unit cell
$v_{(\alpha\beta\gamma)}^{(pqr)}$	volume of the subcell $(\alpha\beta\gamma)$ in the (p, q, r)th unit cell
$\bar{x}_1^{(\alpha)}, \bar{x}_2^{(\beta)}, \bar{x}_3^{(\gamma)}$	local subcell coordinates
$k_i^{(\alpha\beta\gamma)}$	coefficients of heat conductivity of the material in the subcell $(\alpha\beta\gamma)$
$T^{(\alpha\beta\gamma)}$	temperature field in the subcell $(\alpha\beta\gamma)$
$T_{(l,m,n)}^{(\alpha\beta\gamma)}$	temperature at the center of the subcell $(\alpha\beta\gamma)$ when $l = m = n = 0$; coefficients associated with higher-order terms in the temperature field expansion within the subcell $(\alpha\beta\gamma)$ for other values of l, m, n
$q_i^{(\alpha\beta\gamma)}$	components of the heat flux vector in the subcell $(\alpha\beta\gamma)$
$Q_{(l,m,n)}^{(\alpha\beta\gamma)}$	average values of the subcell heat flux component $q_1^{(\alpha\beta\gamma)}$ when $l = m = n = 0$; higher-order heat fluxes for other values of l, m, n
$L_{(l,m,n)}^{(\alpha\beta\gamma)}$	surface integrals of subcell interfacial heat fluxes
$u_i^{(\alpha\beta\gamma)}$	displacement components in the subcell $(\alpha\beta\gamma)$
$W_{(l,m,n)}^{(\alpha\beta\gamma)}$	displacement components at the center of the subcell $(\alpha\beta\gamma)$ when $l = m = n = 0$; coefficients associated with higher-order terms in the displacement field expansion within the subcell $(\alpha\beta\gamma)$ for other values of l, m, n
$\varepsilon_{ij}^{(\alpha\beta\gamma)}$	local strain components in the subcell $(\alpha\beta\gamma)$
$\sigma_{ij}^{(\alpha\beta\gamma)}$	local stress components in the subcell $(\alpha\beta\gamma)$
$c_{ijkl}^{(\alpha\beta\gamma)}$	elements of stiffness tensor of the material in the subcell $(\alpha\beta\gamma)$
$\Gamma_{ij}^{(\alpha\beta\gamma)}$	elements of the thermal tensor of the material in the subcell $(\alpha\beta\gamma)$
$S_{ij(l,m,n)}^{(\alpha\beta\gamma)}$	average values of the subcell stress components $\sigma_{ij}^{(\alpha\beta\gamma)}$ when $l = m = n = 0$; higher-order stress components for other values of l, m, n

† On leave from the Faculty of Engineering, Tel-Aviv University, Ramat-Aviv 69978, Israel.

$I^{(\alpha\beta_c)}_{1f(n,0,0)}$ surface integrals of the subcell interfacial stresses $\sigma^{(\alpha\beta_c)}_{1f}$ at $\bar{x}^{(\alpha)}_1 = \pm d_c/2$

$J^{(\alpha\beta_c)}_{2f(0,n,0)}$ surface integrals of the subcell interfacial stresses $\sigma^{(\alpha\beta_c)}_{2f}$ at $\bar{x}^{(\beta)}_2 = \pm h^{(q)}_\beta/2$

$K^{(\alpha\beta_c)}_{3f(0,0,n)}$ surface integrals of the subcell interfacial stresses $\sigma^{(\alpha\beta_c)}_{3f}$ at $\bar{x}^{(\gamma)}_3 = \pm l^{(r)}_\gamma/2$

1. INTRODUCTION

Functionally graded materials (FGMs) are a new generation of composite materials in which the microstructural details are spatially varied through nonuniform distribution of the reinforcement phase, by using reinforcement with different properties, sizes and shapes, as well as by interchanging the roles of reinforcement and matrix phases in a continuous manner. The result is a microstructure that produces continuously changing thermal and mechanical properties at the macroscopic or continuum level.

The use of functionally graded materials in applications involving severe thermal gradients is quickly gaining acceptance in the composite mechanics community and the aerospace and aircraft industry. This is particularly true in Japan and Europe, where the concept of FGMs was conceived. The current approach employed by the Japanese and European researchers in analyzing the response of FGMs to thermal gradients is the standard micromechanics approach based on the concept of a representative volume element (RVE) assumed to be definable at each point within the heterogeneous material (cf. Wakashima and Tsukamoto, 1990; Fukushima, 1992). This assumption, however, neglects the possibility of coupling between local and global effects, thus leading to potentially erroneous results in the presence of macroscopically nonuniform material properties and large field variable gradients. This is particularly true when the temperature gradient is large with respect to the dimension of the inclusion phase, the characteristic dimension of the inclusion phase is large relative to the global dimensions of the composite, and the number of uniformly or nonuniformly distributed inclusions is relatively small (Aboudi *et al.*, 1993). Perhaps the most important objection to using the standard RVE-based micromechanics approach in the analysis of FGMs is the lack of a theoretical basis for the definition of an RVE, which clearly *cannot be unique in the presence of continuously changing properties owing to nonuniform inclusion spacing.*

As a result of the limitations and shortcomings of the standard micromechanics approach, a new higher order micromechanical theory for functionally graded materials, "HOTFGM", that explicitly couples the local and global effects, has been developed (Aboudi *et al.*, 1993; Aboudi *et al.*, 1994a,b). The results obtained thus far have demonstrated that the theory is an accurate, efficient and viable tool in the analysis of functionally graded materials and design of functionally graded architectures in metal matrix composites. These results include verification of the accuracy of HOTFGM using the finite-element method (Pindera and Dunn, 1995), and the assessment of the applicability of the uncoupled micromechanics approach for the analysis of functionally graded materials (Pindera *et al.*, 1994, 1995). In particular, comparison of results obtained using the standard micromechanics approach with those of HOTFGM has demonstrated the need for a theory which explicitly takes into account the micro-macrostructural coupling effects, thus justifying the development of the coupled higher-order theory.

HOTFGM is a recently constructed theory that continues to evolve. The original formulation has been developed in the Cartesian coordinate system, and was intended for the analysis of functionally graded plates subjected to a temperature gradient across the plate's thickness that coincides with the direction along which the microstructure is graded. The most recent developments of the Cartesian-based theory include incorporation of two inelastic constitutive models for the response of metallic matrices (Aboudi *et al.*, 1995a) and extension of the theoretical framework to include generalized plane strain loading situations in order to facilitate modeling of actual functionally graded structural components (Aboudi *et al.*, 1995b).

In this paper we present a further extension of HOTFGM that involves development of a two-dimensional framework to enable modeling of composites functionally graded in two directions. The analytical approach in the two-dimensional theory, as in the one-dimensional version, is based on volumetric averaging of the various field quantities together

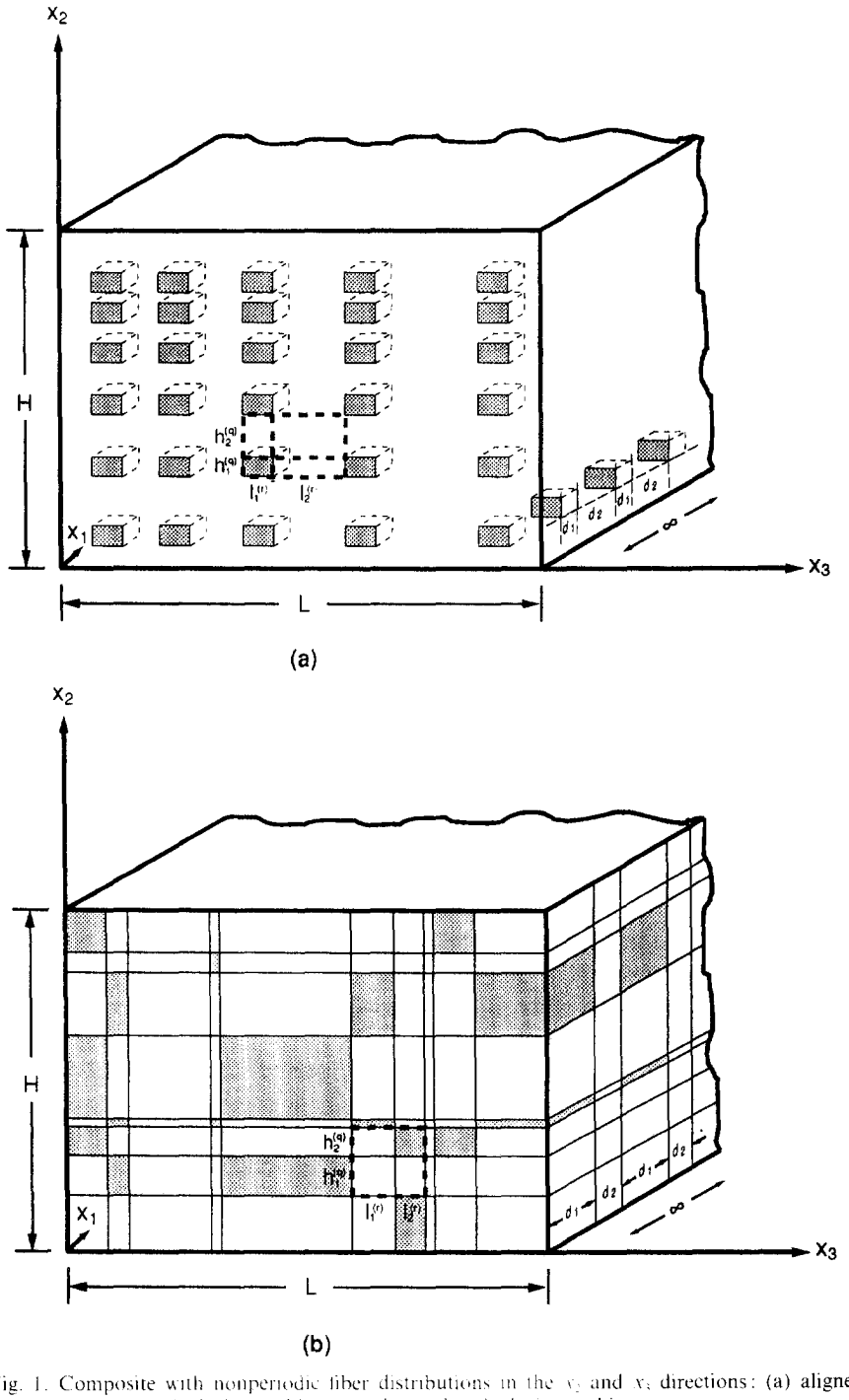

Fig. 1. Composite with nonperiodic fiber distributions in the x_2 and x_3 directions: (a) aligned inclusion architecture, (b) random inclusion architecture.

with the imposition of boundary and interfacial continuity conditions in an average sense. The previous restriction of periodicity in two orthogonal directions, however, is presently abandoned thus allowing arbitrary distribution of one or more reinforcement phases in one plane. This leads to a significant generalization of the theory. As a result, composites with finite dimensions along the functionally graded directions can be analysed. Figure 1 illustrates the types of internal architectures that can be analysed with this new two-dimensional version of HOTFGM. These architectures include rows of aligned inclusions (or continuous fibers) with variable spacing in the functionally graded x_2 and x_3 directions and regular spacing in the periodic x_1 direction (Fig. 1a). Alternatively, completely random

inclusion (or fiber) architectures in the x_2–x_3 plane can also be admitted (Fig. 1b). At present, the two-dimensional version of the theory, herein called HOTFGM-2D, is limited to the analysis of functionally graded composites in the linearly elastic range.

This theory is subsequently employed to study the free-edge problem in a symmetrically laminated B/Ep–Ti composite plate subjected to a uniform temperature change. The capability of the theory to capture large stress gradients near a geometric discontinuity such as the free edge is established upon comparison with finite-element analysis carried out by Herakovich (1976) using homogenized properties for the B/Ep plies. Subsequent incorporation of the actual microstructure of the B/Ep plies in the HOTFGM-2D analysis of the free-edge stress fields demonstrates the limitations of the homogenized continuum approach in the presence of course microstructure and large stress gradients. Finally, the potential of using functionally graded fiber architectures in reducing edge effects in laminated MMC plates is demonstrated by investigating the effect of nonuniform fiber distributions in the B/Ep plies near the free edge. It should be noted that even though the utility of the theory is demonstrated herein for the special case of a symmetric laminate under uniform temperature change, the theory naturally can be employed in more complicated situations with non-zero temperature gradients.

2. ANALYTICAL MODEL

HOTFGM-2D is based on the geometric model of a heterogeneous composite with a finite thickness H, and finite length L, that is infinite in the x_1 direction (see Fig. 1). The loading applied to the boundaries of the composite in the x_2–x_3 plane may involve an arbitrary temperature distribution and mechanical effects represented by a combination of surface displacements and/or tractions. The composite is reinforced in the x_2–x_3 plane by an arbitrary distribution of infinitely long fibers oriented along the x_1 axis, or finite-length inclusions that are arranged in a periodic manner in the direction of the x_1 axis. The heterogeneous composite is constructed using a basic building block (p, q, r) (Fig. 2a), consisting of eight subcells designated by the triplet $(\alpha\beta\gamma)$, (Fig. 2b). Each index α, β, γ takes on the values 1 or 2 which indicate the relative position of the given subcell along the x_1, x_2 and x_3 axes, respectively. The dimensions of the unit cell along the x_1 axis, d_1, d_2, are fixed for the given configuration since this is the periodic direction, whereas the dimensions along the x_2 and x_3 axes or the FG directions, $h_1^{(q)}$, $h_2^{(q)}$, and $l_1^{(r)}$, $l_2^{(r)}$, can vary from unit cell to unit cell. The dimensions of the subcells within a given cell along the FG directions are designated with running indices q and r which identify the cell number in the x_2–x_3 plane, where q and r remain constant along the x_1 axis. For the remaining direction, x_1, the corresponding index p is introduced. Thus a given cell is designated by the triplet (p, q, r) for an infinite range of p owing to periodicity in the x_1 direction, and for $q = 1, 2, \ldots, N_q$ and $r = 1, 2, \ldots, N_r$, where N_q and N_r are the number of cells in the FG x_2 and x_3 directions.

It is important to note that the unit cell (p, q, r) in the present framework is not taken to be an RVE whose effective properties can be obtained through local homogenization, as is done in the standard uncoupled micromechanical approaches based on the concept of *local action* (Malvern, 1969). In fact, for fully nonuniform distributions of fibers or inclusions in the x_2–x_3 plane, no RVE can be identified. Thus the principle of local action is not applicable at the individual cell level, requiring the response of each cell to be explicitly coupled to the response of the entire array of cells in the FG directions. This is what is meant by the statement that the present approach explicitly couples the microstructural details with the global analysis, and thus sets HOTFGM-2D apart from the standard approaches found in the literature. The limitations of the standard uncoupled approach, and the error that results from decoupling of the local and global effects, were recently discussed by Pindera *et al.* (1994, 1995).

2.1. *Outline of the solution technique*

The solution of the thermomechanical boundary-value problem outlined in the foregoing is solved in two steps, following the general framework for the solution of the corresponding one-dimensional thermoelastic problem discussed previously (Aboudi *et al.*,

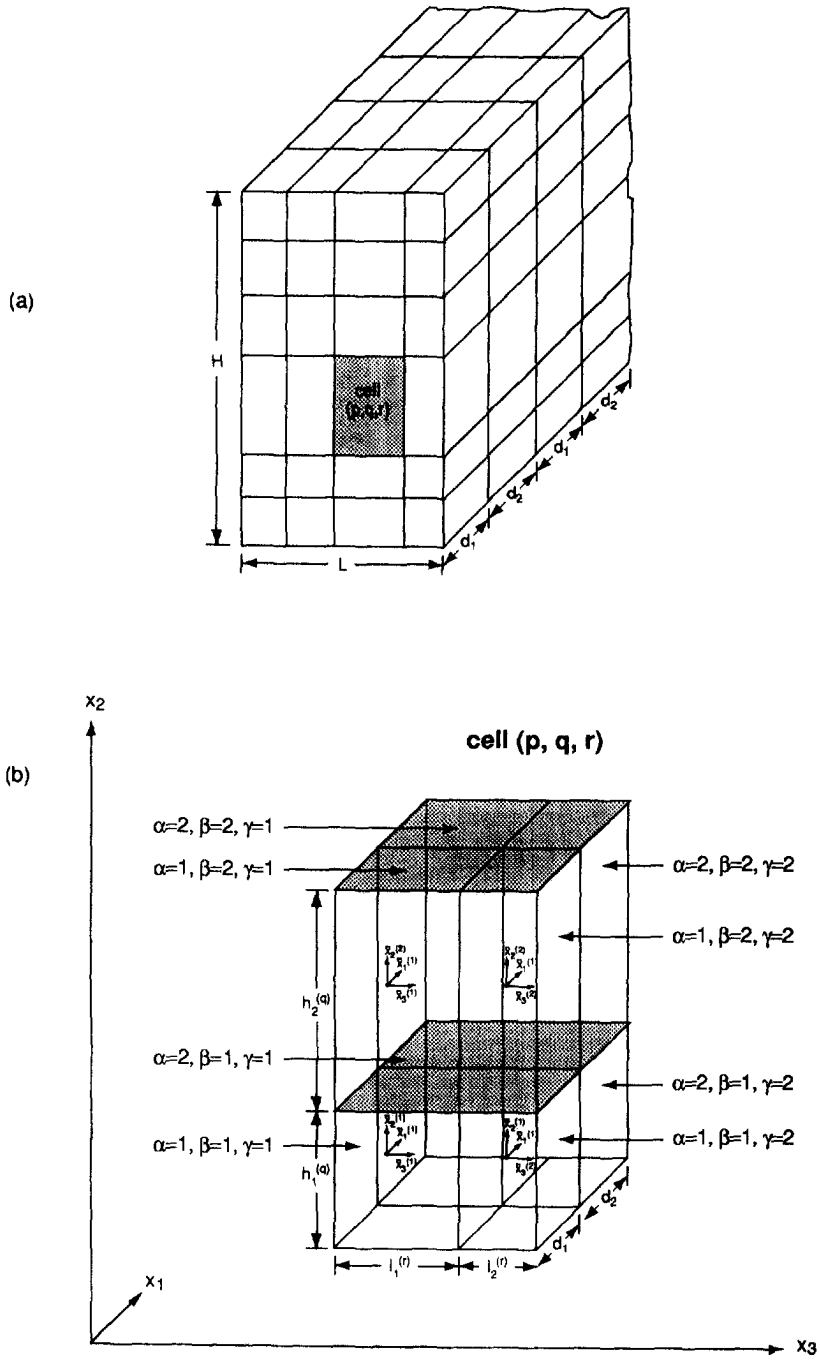

Fig. 2. (a) Three-dimensional schematic of a functionally graded composite in the x_2 and x_3 directions showing the dimensions of the basic building block (b) of the composite.

1993). In the first step, the temperature distribution in every cell is determined by solving the heat equation under steady-state conditions in each cell subject to the appropriate continuity and compatibility conditions. The solution to the heat equation is obtained by approximating the temperature field in each subcell of a unit cell using a quadratic expansion in the local coordinates $\bar{x}^{(2)}$, $\bar{x}^{(1)}$, $\bar{x}^{(3)}$, centered at the subcell's mid-point. A higher-order representation of the temperature field is necessary in order to capture the local effects created by the thermomechanical field gradients, the microstructure of the composite and the finite dimensions in the FG directions, in contrast with previous treatments involving fully periodic composite media which employed linear expansions (Aboudi, 1991). The

unknown coefficients associated with each term in the expansion are then obtained by constructing a system of equations that satisfies the requirements of a standard boundary-value problem for the given temperature field approximation. That is, the heat equation is satisfied in a volumetric sense, and the thermal and heat flux continuity conditions within a given cell, as well as between a given cell and adjacent cells, are imposed in an average sense.

Given the temperature distribution in the functionally graded composite in the periodic and FG directions, internal displacements, strains and stresses are subsequently generated by solving the equilibrium equations in each cell subject to appropriate continuity and boundary conditions. The solution is obtained by approximating the displacement field in the FG directions in each subcell using a quadratic expansion in local coordinates within the subcell. The displacement field in the periodic x_1 direction, on the other hand, is approximated using linear expansion in local coordinates to reflect the periodic character of the composite's microstructure along the x_1 axis. The unknown coefficients associated with each term in the expansion are obtained by satisfying the appropriate field equations in a volumetric sense, together with the boundary conditions and continuity of displacements and tractions between individual subcells of a given cell, and between adjacent cells. The continuity conditions are imposed in an average sense. This results in a coupled system of equations involving the unknown coefficients in the displacement representation for each cell.

An outline of the governing equations for the temperature and displacement fields in the individual subcells within the rows and columns of cells considered in solving the outlined boundary-value problem is given in the following. A detailed derivation of these equations is presented in Appendices A and B so as not to obscure the basic concepts by the involved algebraic manipulations.

2.2. *Thermal analysis: problem formulation*

Suppose that the composite material occupies the region $|x_1| < \infty$, $0 \leqslant x_2 \leqslant H$, $0 \leqslant x_3 \leqslant L$. Let the composite be subjected to the temperature T_T on the top surface ($x_2 = H$), T_B on the bottom surface ($x_2 = 0$), T_L on the left surface ($x_3 = 0$), and T_R on the right surface ($x_3 = L$). Also, let N_q denote the number of cells in the interval $0 \leqslant x_2 \leqslant H$, i.e.

$$H = \sum_{q=1}^{N_q} (h_1^{(q)} + h_2^{(q)}).$$

Likewise, let N_r denote the number of cells in the interval $0 \leqslant x_3 \leqslant L$, i.e.

$$L = \sum_{r=1}^{N_r} (l_1^{(r)} + l_2^{(r)}).$$

For $q = 2, \ldots, N_{q-1}$ and $r = 2, \ldots, N_{r-1}$ the cells are internal, whereas for $q = 1, N_q$ and $r = 1, N_r$ they are boundary cells.

2.2.1. *Heat conduction equation.* For a steady-state situation, the heat flux field in the material occupying the subcell $(\alpha\beta\gamma)$ of the (p, q, r)th cell, in the region defined by $|\bar{x}_1^{(\alpha)}| \leqslant \frac{1}{2}d_\alpha, |\bar{x}_2^{(\beta)}| \leqslant \frac{1}{2}h_\beta^{(q)}, |\bar{x}_3^{(\gamma)}| \leqslant \frac{1}{2}l_\gamma^{(r)}$, must satisfy:

$$\hat{c}_1 q_1^{(\alpha\beta\gamma)} + \hat{c}_2 q_2^{(\alpha\beta\gamma)} + \hat{c}_3 q_3^{(\alpha\beta\gamma)} = 0, \tag{1}$$

where $\hat{c}_1 = \partial/\partial\bar{x}_1^{(\alpha)}$, $\hat{c}_2 = \partial/\partial\bar{x}_2^{(\beta)}$, $\hat{c}_3 = \partial/\partial\bar{x}_3^{(\gamma)}$. The components of the heat flux vector $q_i^{(\alpha\beta\gamma)}$ in this subcell are derived from the temperature field according to:

$$q_i^{(\alpha\beta\gamma)} = -k_i^{(\alpha\beta\gamma)}\partial_i T^{(\alpha\beta\gamma)}, \quad (i = 1, 2, 3; \text{ no sum}), \tag{2}$$

where $k_i^{(\alpha\beta\gamma)}$ are the coefficients of heat conductivity of the material in the subcell $(\alpha\beta\gamma)$, and no summation is implied by repeated Greek letters in the above and henceforth. Given the relation between the heat flux and temperature, a temperature distribution that satisfies the heat conduction equation is sought subject to the continuity and boundary conditions given below.

2.2.2. *Heat flux continuity conditions.* The continuity of the heat flux vector $\mathbf{q}^{(\alpha\beta\gamma)}$ at the interfaces separating adjacent subcells within the unit cell (p, q, r) is fulfilled by imposing the relations

$$q_1^{(\alpha\beta\gamma)}\Big|_{x_1^{(\alpha\beta\gamma)}=d_1^{(\alpha\beta\gamma)}/2} = q_1^{(\alpha+1,\beta,\gamma)}\Big|_{x_1^{(\alpha+1,\beta,\gamma)}=-d_1^{(\alpha+1,\beta,\gamma)}/2} \tag{3a}$$

$$q_2^{(\alpha\beta\gamma)}\Big|_{x_2^{(\alpha\beta\gamma)}=h_2^{(\alpha\beta\gamma)}/2} = q_2^{(\alpha,\beta+1,\gamma)}\Big|_{x_2^{(\alpha,\beta+1,\gamma)}=-h_2^{(\alpha,\beta+1,\gamma)}/2} \tag{3b}$$

$$q_3^{(\alpha\beta\gamma)}\Big|_{x_3^{(\alpha\beta\gamma)}=l_3^{(\alpha\beta\gamma)}/2} = q_3^{(\alpha\beta,\gamma+1)}\Big|_{x_3^{(\alpha\beta,\gamma+1)}=-l_3^{(\alpha\beta,\gamma+1)}/2}. \tag{3c}$$

In addition to the above continuity conditions within the (p, q, r)th cell, the heat flux continuity at the interfaces between neighboring cells must be ensured. The conditions that ensure this are given by

$$q_1^{(\alpha\beta\gamma)}\Big|_{x_1^{(\alpha\beta\gamma)}=d_1^{(\alpha\beta\gamma)}/2} = q_1^{(\alpha+1,\beta,\gamma)}\Big|_{x_1^{(\alpha+1,\beta,\gamma)}=-d_1^{(\alpha+1,\beta,\gamma)}/2} \tag{4a}$$

$$q_2^{(\alpha\beta\gamma)}\Big|_{x_2^{(\alpha\beta\gamma)}=h_2^{(\alpha\beta\gamma)}/2} = q_2^{(\alpha,\beta+1,\gamma)}\Big|_{x_2^{(\alpha,\beta+1,\gamma)}=-h_2^{(\alpha,\beta+1,\gamma)}/2} \tag{4b}$$

$$q_3^{(\alpha\beta\gamma)}\Big|_{x_3^{(\alpha\beta\gamma)}=l_3^{(\alpha\beta\gamma)}/2} = q_3^{(\alpha\beta,\gamma+1)}\Big|_{x_3^{(\alpha\beta,\gamma+1)}=-l_3^{(\alpha\beta,\gamma+1)}/2}. \tag{4c}$$

2.2.3. *Thermal continuity conditions.* The thermal continuity conditions at the interfaces separating adjacent subcells within the cell (p, q, r) are given by relations similar to the corresponding heat flux continuity conditions.

$$T^{(\alpha\beta\gamma)}\Big|_{x_1^{(\alpha\beta\gamma)}=d_1^{(\alpha\beta\gamma)}/2} = T^{(\alpha+1,\beta,\gamma)}\Big|_{x_1^{(\alpha+1,\beta,\gamma)}=-d_1^{(\alpha+1,\beta,\gamma)}/2} \tag{5a}$$

$$T^{(\alpha\beta\gamma)}\Big|_{x_2^{(\alpha\beta\gamma)}=h_2^{(\alpha\beta\gamma)}/2} = T^{(\alpha,\beta+1,\gamma)}\Big|_{x_2^{(\alpha,\beta+1,\gamma)}=-h_2^{(\alpha,\beta+1,\gamma)}/2} \tag{5b}$$

$$T^{(\alpha\beta\gamma)}\Big|_{x_3^{(\alpha\beta\gamma)}=l_3^{(\alpha\beta\gamma)}/2} = T^{(\alpha\beta,\gamma+1)}\Big|_{x_3^{(\alpha\beta,\gamma+1)}=-l_3^{(\alpha\beta,\gamma+1)}/2}. \tag{5c}$$

while the thermal continuity at the interfaces between neighboring cells is ensured, as in the case of the heat flux field, by requiring that

$$T^{(\alpha\beta\gamma)}\Big|_{x_1^{(\alpha\beta\gamma)}=d_1^{(\alpha\beta\gamma)}/2} = T^{(\alpha+1,\beta,\gamma)}\Big|_{x_1^{(\alpha+1,\beta,\gamma)}=-d_1^{(\alpha+1,\beta,\gamma)}/2} \tag{6a}$$

$$T^{(\alpha\beta\gamma)}\Big|_{x_2^{(\alpha\beta\gamma)}=h_2^{(\alpha\beta\gamma)}/2} = T^{(\alpha,\beta+1,\gamma)}\Big|_{x_2^{(\alpha,\beta+1,\gamma)}=-h_2^{(\alpha,\beta+1,\gamma)}/2} \tag{6b}$$

$$T^{(\alpha\beta\gamma)}\Big|_{x_3^{(\alpha\beta\gamma)}=l_3^{(\alpha\beta\gamma)}/2} = T^{(\alpha\beta,\gamma+1)}\Big|_{x_3^{(\alpha\beta,\gamma+1)}=-l_3^{(\alpha\beta,\gamma+1)}/2}. \tag{6c}$$

2.2.4. *Boundary conditions.* The final set of conditions that the solution for the temperature field must satisfy are the boundary conditions at the top and bottom, and left and right surfaces. The temperature in the cell $(p, 1, r)$ at the bottom surface must equal the applied temperature T_B, whereas in the cell (p, N_q, r) at the top surface the temperature must be T_T.

$$T^{(\alpha\beta\gamma)}|^{(p,q,1)} = T_B(x_3), \quad \bar{x}_3^{(1)} = -\tfrac{1}{2}h_1^{(1)} \tag{7a}$$

$$T^{(\alpha\beta\gamma)}|^{(p,q,N_r)} = T_T(x_3), \quad \bar{x}_3^{(2)} = \tfrac{1}{2}h_2^{(N_q)}, \tag{7b}$$

where $r = 1, \ldots, N_r$.

Similarly, the temperature in the cell $(p, q, 1)$ at the left surface must equal the applied temperature T_L, whereas in the cell (p, q, N_r) at the right surface the temperature must be T_R.

$$T^{(\alpha\beta\gamma)}|^{(p,q,1)} = T_L(x_2), \quad \bar{x}_3^{(1)} = -\tfrac{1}{2}l_1^{(1)} \tag{8a}$$

$$T^{(\alpha\beta\gamma)}|^{(p,q,N_r)} = T_R(x_2), \quad \bar{x}_3^{(2)} = \tfrac{1}{2}l_2^{(N_r)}, \tag{8b}$$

where $q = 1, \ldots, N_q$.

Alternatively, it is possible to impose mixed-boundary conditions involving temperature and heat flux at different portions of the boundary.

2.3. *Thermal analysis: solution*

The temperature distribution in the subcell $(\alpha\beta\gamma)$ of the (p, q, r)th cell, measured with respect to a reference temperature T_{ref}, is denoted by $T^{(\alpha\beta\gamma)}$. We approximate this temperature field by a second order expansion in the local coordinates $\bar{x}_1^{(\alpha)}$, $\bar{x}_2^{(\beta)}$, and $\bar{x}_3^{(\gamma)}$ as follows:

$$T^{(\alpha\beta\gamma)} = T^{(\alpha\beta\gamma)}_{(000)} + \bar{x}_2^{(\beta)} T^{(\alpha\beta\gamma)}_{(010)} + \bar{x}_3^{(\gamma)} T^{(\alpha\beta\gamma)}_{(001)} + \frac{1}{2}\left(3\bar{x}_1^{(\alpha)2} - \frac{d_\alpha^2}{4}\right) T^{(\alpha\beta\gamma)}_{(200)} + \frac{1}{2}\left(3\bar{x}_2^{(\beta)2} - \frac{h_\beta^{(q)2}}{4}\right) T^{(\alpha\beta\gamma)}_{(020)} + \frac{1}{2}\left(3\bar{x}_3^{(\gamma)2} - \frac{l_\gamma^{(r)2}}{4}\right) T^{(\alpha\beta\gamma)}_{(002)}, \tag{9}$$

where $T^{(\alpha\beta\gamma)}_{(000)}$, which is the temperature at the center of the subcell, and $T^{(\alpha\beta\gamma)}_{(lmn)}$ ($l, m, n = 0, 1$, or 2 with $l+m+n \leqslant 2$) are unknown coefficients which are determined from conditions that will be outlined subsequently. It should be noted that eqn (9) does not contain a linear term in the local coordinates $\bar{x}_1^{(\alpha)}$. This follows directly from the assumed perodicity in the x_1 direction and symmetry with respect to the lines $\bar{x}_1^{(\alpha)} = 0$ for $\alpha = 1$ and 2.

Given the six unknown quantities associated with each subcell (i.e. $T^{(\alpha\beta\gamma)}_{(000)}, \ldots, T^{(\alpha\beta\gamma)}_{(002)}$) and eight subcells within each unit cell, $48N_qN_r$ unknown quantities must be determined for a composite with N_q rows and N_r columns of different materials. These quantities are determined by first satisfying the heat conduction equation, as well as the first and second moment of this equation in each subcell in a volumetric sense in view of the temperature field approximation given by eqn (9). Subsequently, continuity of heat flux and temperature is imposed in an average sense at the interfaces separating adjacent subcells, as well as neighboring cells. Fulfillment of these field equations and continuity conditions, together with the imposed thermal boundary conditions at the top and bottom, and left and right surfaces of the composite, provides the necessary $48N_qN_r$ equations for the $48N_qN_r$ unknown coefficients in the temperature field expansion. We begin the outline of steps to generate the required $48N_qN_r$ equations by first considering an arbitrary (p,q,r)th cell in the interior of the composite (i.e. $q = 2, \ldots, N_q - 1$ and $r = 2, \ldots, N_r - 1$). This produces $48(N_q-2)(N_r-2)$ equations. The additional equations are obtained by considering the boundary cells (i.e. $q = 1, N_q$ and $r = 1, N_r$). For these cells, most of the preceding relations also hold, with the exception of some of the interfacial continuity conditions between adjacent cells which are replaced by the specified boundary conditions.

2.3.1. *Heat conduction equations.*

In the course of satisfying the steady-state heat equation in a volumetric sense, it is convenient to define the following flux quantities:

$$Q_{ilmn}^{(\alpha\beta_\gamma)} = \frac{1}{V_{(\alpha\beta_\gamma)}^{(pqr)}} \int_{x_1^{(p-1)}+d_1^{(\alpha)}}^{x_1^{(p-1)}+d_1^{(\alpha)}+d_1^{(\beta)}} \int_{x_2^{(q-1)}+h_\beta^{(\alpha)}}^{x_2^{(q-1)}+h_\beta^{(\alpha)}+h_\beta^{(\beta)}} \int_{x_3^{(r-1)}+l_\gamma^{(\alpha)}}^{x_3^{(r-1)}+l_\gamma^{(\alpha)}+l_\gamma^{(\beta)}} (\bar{x}_1^{(\alpha)})^i (\bar{x}_2^{(\beta)})^m (\bar{x}_3^{(\gamma)})^n q_i^{(\alpha\beta_\gamma)} \, \mathrm{d}\bar{x}_1^{(\alpha)} \, \mathrm{d}\bar{x}_2^{(\beta)} \, \mathrm{d}\bar{x}_3^{(\gamma)}, \tag{10}$$

where $l, m, n = 0, 1$, or 2 with $l + m + n \leqslant 2$, and $v_{(\alpha\beta_\gamma)}^{(pqr)} = d_\alpha h_\beta^{(\alpha)} l_\gamma^{(\alpha)}$ is the volume of the subcell $(\alpha\beta_\gamma)$ in the (p, q, r)th cell. For $l = m = n = 0$, $Q_{i(0,0,0)}^{(\alpha\beta_\gamma)}$ is the average value of the heat flux component $q_i^{(\alpha\beta_\gamma)}$ in the subcell, whereas for other values of (l, m, n) eqn (10) defines higher-order heat fluxes. These flux quantities can be evaluated explicitly in terms of the coefficients $T_{(lmn)}^{(\alpha\beta_\gamma)}$ by performing the required volume integration using eqns (2) and (9) in (10). This yields the following non-vanishing zeroth-order and first-order heat fluxes in terms of the unknown coefficients in the temperature field expansion.

$$Q_{1(1,0,0)}^{(\alpha\beta_\gamma)} = -k_1^{(\alpha\beta_\gamma)} \frac{d_\alpha}{4} T_{12(0)}^{(\alpha\beta_\gamma)} \tag{11}$$

$$Q_{2(0,0,0)}^{(\alpha\beta_\gamma)} = -k_2^{(\alpha\beta_\gamma)} T_{(0)(0)}^{(\alpha\beta_\gamma)} \tag{12}$$

$$Q_{2(0,1,0)}^{(\alpha\beta_\gamma)} = -k_2^{(\alpha\beta_\gamma)} \frac{h_\beta^{(\alpha\beta_\gamma)}}{4} T_{(0)(2)(0)}^{(\alpha\beta_\gamma)} \tag{13}$$

$$Q_{3(0,0,0)}^{(\alpha\beta_\gamma)} = -k_3^{(\alpha\beta_\gamma)} T_{(0)(0)(1)}^{(\alpha\beta_\gamma)} \tag{14}$$

$$Q_{3(0,0,1)}^{(\alpha\beta_\gamma)} = -k_3^{(\alpha\beta_\gamma)} \frac{l_\gamma^{(\alpha\beta_\gamma)}}{4} T_{(0)(0)(2)}^{(\alpha\beta_\gamma)} \tag{15}$$

Satisfaction of the zeroth, first and second moments of the steady-state heat equation results in the following eight relationships among the first-order heat fluxes $Q_{i(l,m,n)}^{(\alpha\beta_\gamma)}$ in the different subcells $(\alpha\beta_\gamma)$ of the (p, q, r)th cell, after some involved algebraic manipulations (see Appendix A):

$$[Q_{1(1,0,0)}^{(\alpha\beta_\gamma)} d_\alpha^2 + Q_{2(0,1,0)}^{(\alpha\beta_\gamma)} h_\beta^2 + Q_{3(0,0,1)}^{(\alpha\beta_\gamma)} l_\gamma^2]^{(p,q,r)} = 0, \tag{16}$$

where the triplet $(\alpha\beta_\gamma)$ assumes all permutations of the integers 1 and 2.

2.3.2. *Heat flux continuity equations.* The continuity of heat fluxes at the subcell interfaces associated with the periodic x_1 direction, eqn (3a) imposed in an average sense, is ensured by:

$$[Q_{1(1,0,0)}^{(\alpha\beta_\gamma)} d_1 + Q_{1(1,0,0)}^{(\alpha\beta_\gamma)} d_1]^{(p,q,r)} = 0. \tag{17}$$

We note that eqn (4a) that ensures continuity of heat flux in the x_1 direction between neighboring cells is identically satisfied by the chosen temperature field representation owing to the periodicity of the composite in this direction.

The equations that ensure heat flux continuity at the subcell interfaces, as well as between individual cells, associated with the x_2 and x_3 directions, eqns (3b, c) and(4b, c) are given by

$$[-12Q_{2(0,1,0)}^{(\alpha1\beta_\gamma)} h_1 + Q_{2(0,0,0)}^{(\alpha2\beta_\gamma)} - 6Q_{2(0,1,0)}^{(\alpha2\beta_\gamma)} h_2]^{(p,q,r)} - [Q_{2(0,0,0)}^{(\alpha2\beta_\gamma)} + 6Q_{2(0,1,0)}^{(\alpha2\beta_\gamma)} h_2]^{(p,q-1,r)} = 0 \tag{18}$$

$$[-Q_{2(0,0,0)}^{(\alpha1\beta_\gamma)} + \tfrac{1}{2}(Q_{2(0,0,0)}^{(\alpha2\beta_\gamma)} - 6Q_{2(0,1,0)}^{(\alpha2\beta_\gamma)} h_2)]^{(p,q,r)} + \tfrac{1}{2}[Q_{2(0,0,0)}^{(\alpha2\beta_\gamma)} - 6Q_{2(0,1,0)}^{(\alpha2\beta_\gamma)} h_2]^{(p,q-1,r)} = 0 \tag{19}$$

$$[-12Q_{3(0,0,1)}^{(\alpha\beta1\gamma)} l_1 + Q_{3(0,0,0)}^{(\alpha\beta2\gamma)} - 6Q_{3(0,0,1)}^{(\alpha\beta2\gamma)} l_2]^{(p,q,r)} - [Q_{3(0,0,0)}^{(\alpha\beta2\gamma)} + 6Q_{3(0,0,1)}^{(\alpha\beta2\gamma)} l_2]^{(p,q,r-1)} = 0 \tag{20}$$

$$[-Q^{(\alpha\beta 1)}_{3(0,0,0)}+\tfrac{1}{2}(Q^{(\alpha\beta 2)}_{3(0,0,0)}-6Q^{(\alpha\beta 2)}_{3(0,0,1)}/l_2)]^{(p,q,r)}+\tfrac{1}{2}[Q^{(\alpha\beta 2)}_{3(0,0,0)}+6Q^{(\alpha\beta 2)}_{3(0,0,1)}/l_2]^{(p,q,r-1)}=0. \quad (21)$$

Equations (17)–(21) provide us with 20 additional relations among the zeroth-order and first-order heat fluxes. These relations, together with eqn (16), can be expressed in terms of the unknown coefficients $T^{(\alpha\beta\gamma)}_{(lmn)}$ by making use of eqns (11)–(15), providing a total of 28 of the required 48 equations necessary for the determination of these coefficients in the (p, q, r)th cell.

2.3.3. *Thermal continuity equations.* An additional set of 20 equations necessary to determine the unknown coefficients in the temperature field expansion is subsequently generated by the thermal continuity conditions imposed on an average basis at each subcell and cell interface. Imposing the thermal continuity at each subcell interface in the periodic x_1 direction, eqn (5a), we obtain the following conditions for the (p,q,r)th cell:

$$[T^{(1\beta\gamma)}_{(000)}+\tfrac{1}{4}d_1^2T^{(1\beta\gamma)}_{(200)}]^{(p,q,r)}=[T^{(2\beta\gamma)}_{(000)}+\tfrac{1}{4}d_2^2T^{(2\beta\gamma)}_{(200)}]^{(p,q,r)}. \quad (22)$$

We note that the continuity of temperature between neighboring cells in the x_1 direction, eqn (6a), is automatically satisfied by the chosen temperature field representation which reflects the periodic character of the composite in this direction.

The continuity of temperature at the interfaces between the subcells, as well as between the neighboring cells, in the FG directions, eqns (5b,c) and (6b,c), on the other hand, yield

$$[T^{(\alpha 1\gamma)}_{(000)}+\tfrac{1}{2}h_1T^{(\alpha 1\gamma)}_{(010)}+\tfrac{1}{4}h_1^2T^{(\alpha 1\gamma)}_{(020)}]^{(p,q,r)}=[T^{(\alpha 2\gamma)}_{(000)}-\tfrac{1}{2}h_2T^{(\alpha 2\gamma)}_{(010)}+\tfrac{1}{4}h_2^2T^{(\alpha 2\gamma)}_{(020)}]^{(p,q,r)} \quad (23)$$

$$[T^{(\alpha 2\gamma)}_{(000)}+\tfrac{1}{2}h_2T^{(\alpha 2\gamma)}_{(010)}+\tfrac{1}{4}h_2^2T^{(\alpha 2\gamma)}_{(020)}]^{(p,q,r)}=[T^{(\alpha 1\gamma)}_{(000)}-\tfrac{1}{2}h_1T^{(\alpha 1\gamma)}_{(010)}+\tfrac{1}{4}h_1^2T^{(\alpha 1\gamma)}_{(020)}]^{(p,q+1,r)} \quad (24)$$

$$[T^{(\alpha\beta 1)}_{(000)}+\tfrac{1}{2}l_1T^{(\alpha\beta 1)}_{(001)}+\tfrac{1}{4}l_1^2T^{(\alpha\beta 1)}_{(002)}]^{(p,q,r)}=[T^{(\alpha\beta 2)}_{(000)}-\tfrac{1}{2}l_2T^{(\alpha\beta 2)}_{(001)}+\tfrac{1}{4}l_2^2T^{(\alpha\beta 2)}_{(002)}]^{(p,q,r)} \quad (25)$$

$$[T^{(\alpha\beta 2)}_{(000)}+\tfrac{1}{2}l_2T^{(\alpha\beta 2)}_{(001)}+\tfrac{1}{4}l_2^2T^{(\alpha\beta 2)}_{(002)}]^{(p,q,r)}=[T^{(\alpha\beta 1)}_{(000)}-\tfrac{1}{2}l_1T^{(\alpha\beta 1)}_{(001)}+\tfrac{1}{4}l_1^2T^{(\alpha\beta 1)}_{(002)}]^{(p,q,r-1)}. \quad (26)$$

Equations (22)–(26) comprise the required additional 20 relations.

2.3.4. *Governing equations for the unknown coefficients in the temperature expansion.* The steady-state state heat equations, eqn (16), together with the heat flux and thermal continuity equations, eqns (17)–(21) and (22)–(26), respectively, form altogether 48 linear algebraic equations which govern the 48 field variables $T^{(\alpha\beta\gamma)}_{(lmn)}$ in the eight subcells $(\alpha\beta\gamma)$ of an interior cell (p, q, r): $q = 2, \ldots, N_q - 1$, $r = 2, \ldots, N_r - 1$. For the boundary cells $q = 1$, N_q, and $r = 1$, N_r, a different treatment must be applied. For $q = 1$, the governing equations, eqns (16)–(17) and (20)–(26) are operative. Relations (18)–(19), on the other hand, which follow from the continuity of heat flux between a given cell and the preceding one are not applicable. They are replaced by the condition that the heat flux at the interface between subcell $(\alpha 1\gamma)$ and $(\alpha 2\gamma)$ of the cell $(p, 1, r)$ is continuous, as well as the applied temperature relation at the surface $x_2 = 0$, eqn (7a). For the cell $q = N_q$, the previous equations are applicable except eqns (24) which are obviously not operative. These equations are replaced by the specific temperature applied at the surface $x_2 = H$, eqn (7b). Similar reasoning holds for the subcells $r = 1$ and $r = N_r$.

The governing equations at the interior and boundary cells form a system of $48N_qN_r$ linear algebraic equations in the unknown coefficients $T^{(\alpha\beta\gamma)}_{(lmn)}$. Their solution determines the temperature distribution within the FG composite subjected to the boundary conditions (7) and (8). The final form of this system of equations is symbolically represented below

$$\boldsymbol{\kappa}\mathbf{T} = \mathbf{t}. \quad (27)$$

where the structural thermal conductivity matrix $\boldsymbol{\kappa}$ contains information on the geometry

and thermal conductivities of the individual subcells $(\alpha\beta\gamma)$ in the $N_q N_r$ cells spanning the x_2 and x_3 FG directions, the thermal coefficient vector $\mathbf{T}$ contains the unknown coefficients that describe the thermal field in each subcell, i.e. $\mathbf{T} = [\mathbf{T}^{(111)}_{(lmn)}, \ldots, \mathbf{T}^{(222)}_{(lmn)}]$ where $\mathbf{T}^{(\alpha\beta\gamma)}_{(lmn)} = [T_{(000)}, T_{(010)}, T_{(001)}, T_{(200)}, T_{(020)}, T_{(002)}]^{(\alpha\beta\gamma)}$, and the thermal force vector $\mathbf{t}$ contains information on the boundary conditions.

2.4. *Mechanical analysis: problem formulation*

Given the temperature field generated by the applied temperatures T_T, T_B, and T_L, T_R obtained in the preceding section, we proceed to determine the resulting displacement and stress fields. This is carried out for arbitrary mechanical loading applied to the surfaces of the composite in the x_2–x_3 plane, excluding shearing in the x_1 direction.

2.4.1. *Equations of equilibrium.* The stress field in the subcell $(\alpha\beta\gamma)$ of the (p,q,r)th cell generated by the given temperature field must satisfy the equilibrium equations

$$\hat{c}_1 \sigma_{1j}^{(\alpha\beta\gamma)} + \hat{c}_2 \sigma_{2j}^{(\alpha\beta\gamma)} + \hat{c}_3 \sigma_{3j}^{(\alpha\beta\gamma)} = 0, \quad j = 1, 2, 3. \tag{28}$$

where the operator $\hat{c}_i$ has been defined previously. The components of the stress tensor, assuming that the material occupying the subcell $(\alpha\beta\gamma)$ of the (p, q, r)th cell is orthotropic, are related to the strain components through the familiar generalized Hooke's law:

$$\sigma_{ij}^{(\alpha\beta\gamma)} = c_{ijkl}^{(\alpha\beta\gamma)} \varepsilon_{kl}^{(\alpha\beta\gamma)} - \Gamma_{ij}^{(\alpha\beta\gamma)} T^{(\alpha\beta\gamma)}. \tag{29}$$

where $c_{ijkl}^{(\alpha\beta\gamma)}$ are the elements of the stiffness tensor and the elements $\Gamma_{ij}^{(\alpha\beta\gamma)}$ of the so-called thermal tensor are the products of the stiffness tensor and the thermal expansion coefficients. The components of the strain tensor in the individual subcells are, in turn, obtained from the strain–displacement relations

$$\varepsilon_{ij}^{(\alpha\beta\gamma)} = \frac{1}{2}(\hat{c}_j u_i^{(\alpha\beta\gamma)} + \hat{c}_i u_j^{(\alpha\beta\gamma)}), \quad i, j = 1, 2, 3. \tag{30}$$

Given the relation between stresses and displacement gradients obtained from eqns (29) and (30), a displacement field is sought that satisfies the three equilibrium equations together with the continuity and boundary conditions that follow.

2.4.2. *Traction continuity conditions.* The continuity of tractions at the interfaces separating adjacent subcells within the unit cell (p, q, r) is fulfilled by requiring that

$$\sigma_{2j}^{(\alpha\beta\gamma)}\big|_{x_2^{(\alpha)} = h_2^{(p)}} = \sigma_{2j}^{(\alpha+1,\beta\gamma)}\big|_{x_2^{(\alpha+1)} = h_2^{(p)}}, \tag{31a}$$

$$\sigma_{2j}^{(\alpha\beta\gamma)}\big|_{x_2^{(\beta)} = h_3^{(q)}} = \sigma_{2j}^{(\alpha,\beta+1,\gamma)}\big|_{x_3^{(\beta+1)} = h_3^{(q)}}, \tag{31b}$$

$$\sigma_{3j}^{(\alpha\beta\gamma)}\big|_{x_3^{(\gamma)} = h_4^{(r)}} = \sigma_{3j}^{(\alpha\beta,\gamma+1)}\big|_{x_4^{(\gamma+1)} = h_4^{(r)}}. \tag{31c}$$

In addition to the above continuity conditions within the (p, q, r)th cell, the traction continuity at the interfaces between neighboring cells must be ensured. These conditions are fulfilled by requiring that

$$\sigma_{1j}^{(1\beta\gamma)}\big|_{x_2^{(1)} = h_2^{(p+1)}, q, r} = \sigma_{1j}^{(2\beta\gamma)}\big|_{x_2^{(2)} = h_2^{(p)}, q, r}, \tag{32a}$$

$$\sigma_{2j}^{(\alpha 1\gamma)}\big|_{x_2^{(\alpha)} = h_2^{(p)}, q+1, r} = \sigma_{2j}^{(\alpha 2\gamma)}\big|_{x_2^{(\alpha)} = h_2^{(p)}, q, r}, \tag{32b}$$

$$\sigma_{3j}^{(\alpha\beta 1)}\big|_{x_2^{(\alpha)} = h_2^{(p)}, q, r+1} = \sigma_{3j}^{(\alpha\beta 2)}\big|_{x_2^{(\alpha)} = h_2^{(p)}, q, r}. \tag{32c}$$

2.4.3. *Displacement continuity conditions.* At the interfaces of the subcells within the unit cell (p, q, r) the displacements $\mathbf{u} = (u_1, u_2, u_3)$ must be continuous,

$$\mathbf{u}^{(\alpha\beta_\gamma)}\big|^{(p,q,r)}_{\bar{x}_1^{(\alpha)}=d_\alpha/2} = \mathbf{u}^{(\beta\gamma)}\big|^{(p,q,r)}_{\bar{x}_1^{(\alpha)}=-d_\alpha/2} \tag{33a}$$

$$\mathbf{u}^{(\alpha\beta_\gamma)}\big|^{(p,q,r)}_{\bar{x}_2^{(\beta)}=h_\beta^{(q)}/2} = \mathbf{u}^{(\alpha\beta_\gamma)}\big|^{(p,q,r)}_{\bar{x}_2^{(\beta)}=-h_\beta^{(q)}/2} \tag{33b}$$

$$\mathbf{u}^{(\alpha\beta\gamma)}\big|^{(p,q,r)}_{\bar{x}_3^{(\gamma)}=l_\gamma^{(r)}/2} = \mathbf{u}^{(\alpha\beta\gamma)}\big|^{(p,q,r)}_{\bar{x}_3^{(\gamma)}=-l_\gamma^{(r)}/2}, \tag{33c}$$

while the continuity of displacements between neighboring cells is ensured by requiring that

$$\mathbf{u}^{(\alpha\beta_\gamma)}\big|^{(p+1,q,r)}_{\bar{x}_1^{(\alpha)}=-d_\alpha/2} = \mathbf{u}^{(\alpha\beta_\gamma)}\big|^{(p,q,r)}_{\bar{x}_1^{(\alpha)}=d_\alpha/2} \tag{34a}$$

$$\mathbf{u}^{(\alpha\beta_\gamma)}\big|^{(p,q+1,r)}_{\bar{x}_2^{(\beta)}=-h_\beta^{(q+1)}/2} = \mathbf{u}^{(\alpha\beta_\gamma)}\big|^{(p,q,r)}_{\bar{x}_2^{(\beta)}=h_\beta^{(q)}/2} \tag{34b}$$

$$\mathbf{u}^{(\alpha\beta\gamma)}\big|^{(p,q,r+1)}_{\bar{x}_3^{(\gamma)}=-l_\gamma^{(r+1)}/2} = \mathbf{u}^{(\alpha\beta\gamma)}\big|^{(p,q,r)}_{\bar{x}_3^{(\gamma)}=l_\gamma^{(r)}/2}. \tag{34c}$$

2.4.4. Boundary conditions. The final set of conditions that the solution for the displacement field must satisfy are the boundary conditions at the top and bottom, and left and right surfaces. The traction vector in the cells $(p, 1, r)$ and (p, N_q, r) at the bottom and top surfaces, respectively, must equal the applied surface loads,

$$\sigma_{2i}^{(\alpha\beta_\gamma)}\big|^{(p,1,r)} = f_{\mathrm{B}i}(x_3), \quad \bar{x}_2^{(1)} = -\tfrac{1}{2}h_1^{(1)} \tag{35a}$$

$$\sigma_{2i}^{(\alpha\beta_\gamma)}\big|^{(p,N_q,r)} = f_{\mathrm{T}i}(x_3), \quad \bar{x}_2^{(2)} = \tfrac{1}{2}h_2^{(N_q)} \tag{35b}$$

where $r = 1, \ldots, N_r$, $f_{\mathrm{T}i}$ and $f_{\mathrm{B}i}$ describe the spatial variation of these loads at the top and bottom surfaces. Similarly, if the right or left surfaces are rigidly clamped (say), then

$$u_i^{(\alpha\beta\gamma)}\big|^{(p,q,1)} = 0, \quad \bar{x}_3^{(1)} = -\tfrac{1}{2}l_1^{(1)} \tag{36a}$$

$$u_i^{(\alpha\beta\gamma)}\big|^{(p,q,N_r)} = 0, \quad \bar{x}_3^{(2)} = \tfrac{1}{2}l_2^{(N_r)}, \tag{36b}$$

where $q = 1, \ldots, N_q$.
For other types of boundary conditions, eqns (35)–(36) should be modified accordingly.

2.5. *Mechanical analysis: solution*

Owing to symmetry considerations, the displacement field in the subcell $(\alpha\beta\gamma)$ of the (p, q, r)th cell is approximated by a second-order expansion in the local coordinates $\bar{x}_1^{(\alpha)}$, $\bar{x}_2^{(\beta)}$, and $\bar{x}_3^{(\gamma)}$ as follows:

$$u_1^{(\alpha\beta_\gamma)} = \bar{x}_1^{(\alpha)} W_{1(100)}^{(\alpha\beta_\gamma)}$$

$$u_2^{(\alpha\beta_\gamma)} = W_{2(000)}^{(\alpha\beta_\gamma)} + \bar{x}_2^{(\beta)} W_{2(010)}^{(\alpha\beta_\gamma)} + \bar{x}_3^{(\gamma)} W_{2(001)}^{(\alpha\beta_\gamma)} + \tfrac{1}{2}(3\bar{x}_1^{(\alpha)2} - \tfrac{1}{4}d_\alpha^2) W_{2(200)}^{(\alpha\beta_\gamma)}$$
$$+ \tfrac{1}{2}(3\bar{x}_2^{(\beta)2} - \tfrac{1}{4}h_\beta^{(q)2}) W_{2(020)}^{(\alpha\beta_\gamma)} + \tfrac{1}{2}(3\bar{x}_3^{(\gamma)2} - \tfrac{1}{4}l_\gamma^{(r)2}) W_{2(002)}^{(\alpha\beta\gamma)}$$

$$u_3^{(\alpha\beta_\gamma)} = W_{3(000)}^{(\alpha\beta_\gamma)} + \bar{x}_2^{(\beta)} W_{3(010)}^{(\alpha\beta_\gamma)} + \bar{x}_3^{(\gamma)} W_{3(001)}^{(\alpha\beta_\gamma)} + \tfrac{1}{2}(3\bar{x}_1^{(\alpha)2} - \tfrac{1}{4}d_\alpha^2) W_{3(200)}^{(\alpha\beta_\gamma)}$$
$$+ \tfrac{1}{2}(3\bar{x}_2^{(\beta)2} - \tfrac{1}{4}h_\beta^{(q)2}) W_{3(020)}^{(\alpha\beta_\gamma)} + \tfrac{1}{2}(3\bar{x}_3^{(\gamma)2} - \tfrac{1}{4}l_\gamma^{(r)2}) W_{3(002)}^{(\alpha\beta\gamma)}, \tag{37}$$

where $W_{i(000)}^{(\alpha\beta_\gamma)}$, which are the displacements at the center of the subcell, and $W_{i(lmn)}^{(\alpha\beta_\gamma)}$ $(i = 1, 2, 3)$ must be determined from conditions similar to those employed in the thermal problem. In

this case, there are 104 unknown quantities in the (p, q, r)th cell. The determination of these quantities parallels that of the thermal problem. Here, the heat conduction equation is replaced by the three equilibrium equations, and the continuity of tractions and displacements at the various interfaces replaces the continuity of heat fluxes and temperature. Finally, the boundary conditions involve the appropriate mechanical quantities. As in the thermal problem, we start with the internal cells and subsequently modify the governing equations to accommodate the boundary cells $q = 1, N_q$, and $r = 1, N_r$.

It should be noted that the first equation in (37) does not contain linear terms in the local coordinates $\bar{x}_2^{(\beta)}$ and $\bar{x}_3^{(\gamma)}$. This follows from the assumed periodicity in the x_1 direction and symmetry with respect to $\bar{x}_1^{(\alpha)} = 0 (\alpha = 1,2)$. Furthermore, the absence of a constant term in the first equation that represents subcell center x_1-displacements, say $W_{1(000)}^{(\alpha\beta\gamma)}$, leads to the result that the average normal strain of the composite associated with the x_1 direction is zero. It is possible to generalize the present theory by including subcell center displacements associated with the x_1 direction that produce uniform composite strain $\bar{\varepsilon}_{11}$. This generalization leads to an overall behavior of a composite, functionally graded in the x_2 and x_3 directions, that can be described as a generalized plane strain in the x_1 direction. This generalization is not trivial as it requires coupling between the present higher-order theory and an RVE-based theory which employs a homogenization scheme (Aboudi *et al.*, 1995b). In Section 2.5.5 we briefly outline how the present formulation can be modified to admit generalized plane strain in the x_1 direction in order to be able to carry out comparison between HOTFGM-2D and finite-element analysis.

2.5.1. *Equations of equilibrium.* In the course of satisfying the equilibrium equations in a volumetric sense, it is convenient to define the following stress quantities:

$$S_{ij(l,m,n)}^{(\alpha\beta\gamma)} = \frac{1}{V_{(\alpha\beta\gamma)}^{(pqr)}} \int_{-d_\gamma/2}^{d_\gamma/2} \int_{-h_\beta^{(q)}/2}^{h_\beta^{(q)}/2} \int_{-l^{(r)}/2}^{l^{(r)}/2} (\bar{x}_1^{(\alpha)})^l (\bar{x}_2^{(\beta)})^m (\bar{x}_3^{(\gamma)})^n \sigma_{ij}^{(\alpha\beta\gamma)} \, \mathrm{d}\bar{x}_1^{(\alpha)} \, \mathrm{d}\bar{x}_2^{(\beta)} \, \mathrm{d}\bar{x}_3^{(\gamma)}. \tag{38}$$

For $l = m = n = 0$, eqn (38) provides average stresses in the subcell, whereas for other values of (l, m, n) higher-order stresses are obtained that are needed to describe the governing field equations of the higher-order continuum. These stress quantities can be evaluated explicitly in terms of the unknown coefficients $W_{i(lmn)}^{(\alpha\beta\gamma)}$ by performing the required volume integration using eqns (29), (30) and (37) in eqn (38). This yields the following non-vanishing zeroth-order and first-order stress components in terms of the unknown coefficients in the displacement field expansion:

$$S_{11(0,0,0)}^{(\alpha\beta\gamma)} = c_{11}^{(\alpha\beta\gamma)} W_{1(100)}^{(\alpha\beta\gamma)} + c_{12}^{(\alpha\beta\gamma)} W_{2(010)}^{(\alpha\beta\gamma)} + c_{13}^{(\alpha\beta\gamma)} W_{3(001)}^{(\alpha\beta\gamma)} - \Gamma_1^{(\alpha\beta\gamma)} T_{(000)}^{(\alpha\beta\gamma)} \tag{39}$$

$$S_{11(0,1,0)}^{(\alpha\beta\gamma)} = \tfrac{1}{4} h_\beta^{(q)2} c_{12}^{(\alpha\beta\gamma)} W_{2(020)}^{(\alpha\beta\gamma)} - \tfrac{1}{12} h_\beta^{(q)2} \Gamma_1^{(\alpha\beta\gamma)} T_{(010)}^{(\alpha\beta\gamma)} \tag{40}$$

$$S_{11(0,0,1)}^{(\alpha\beta\gamma)} = \tfrac{1}{4} l^{(r)2} c_{13}^{(\alpha\beta\gamma)} W_{3(002)}^{(\alpha\beta\gamma)} - \tfrac{1}{12} l^{(r)2} \Gamma_1^{(\alpha\beta\gamma)} T_{(001)}^{(\alpha\beta\gamma)} \tag{41}$$

with similar expressions for $S_{22(0,0,0)}^{(\alpha\beta\gamma)}$, $S_{22(0,1,0)}^{(\alpha\beta\gamma)}$, $S_{22(0,0,1)}^{(\alpha\beta\gamma)}$ and $S_{33(0,0,0)}^{(\alpha\beta\gamma)}$, $S_{33(0,1,0)}^{(\alpha\beta\gamma)}$, $S_{33(0,0,1)}^{(\alpha\beta\gamma)}$, and

$$S_{12(1,0,0)}^{(\alpha\beta\gamma)} = \tfrac{1}{4} d_\gamma^2 c_{44}^{(\alpha\beta\gamma)} W_{2(100)}^{(\alpha\beta\gamma)} \tag{42}$$

$$S_{13(1,0,0)}^{(\alpha\beta\gamma)} = \tfrac{1}{4} d_\gamma^2 c_{55}^{(\alpha\beta\gamma)} W_{3(100)}^{(\alpha\beta\gamma)} \tag{43}$$

$$S_{23(0,0,0)}^{(\alpha\beta\gamma)} = c_{66}^{(\alpha\beta\gamma)} (W_{2(001)}^{(\alpha\beta\gamma)} + W_{3(010)}^{(\alpha\beta\gamma)}) \tag{44}$$

$$S_{23(0,1,0)}^{(\alpha\beta\gamma)} = \tfrac{1}{4} h_\beta^{(q)2} c_{66}^{(\alpha\beta\gamma)} W_{3(020)}^{(\alpha\beta\gamma)} \tag{45}$$

$$S^{(\alpha\beta\gamma)}_{2j(0,0,1)} = \tfrac{1}{4} l_\gamma^{(r)2} c^{(\alpha\beta\gamma)}_{66} W^{(\alpha\beta\gamma)}_{2(002)}. \tag{46}$$

Satisfaction of the equilibrium equations results in the following sixteen relations among the volume-averaged first-order stresses $S^{(\alpha\beta\gamma)}_{ij(l,m,n)}$ in the different subcells $(\alpha\beta\gamma)$ of the (p, q, r)th cell, after lengthy algebraic manipulations (see Appendix B):

$$[S^{(\alpha\beta\gamma)}_{1j(1,0,0)} d_\alpha^2 + S^{(\alpha\beta\gamma)}_{2j(0,1,0)} h_\beta^2 + S^{(\alpha\beta\gamma)}_{3j(0,0,1)} l_\gamma^2]^{(p,q,r)} = 0, \tag{47}$$

where $j = 2, 3$ and, as in the case of eqn (16), the triplet $(\alpha\beta\gamma)$ assumes all permutations of the integers 1 and 2.

2.5.2. *Traction continuity equations.* The continuity of tractions at the subcell interfaces associated with the periodic x_1 direction, eqn (31a) imposed in an average sense, is ensured by the following relations:

$$[S^{(1\beta\gamma)}_{11(0,0,0)} - S^{(2\beta\gamma)}_{11(0,0,0)}]^{(p,q,r)} = 0 \tag{48}$$

$$[S^{(1\beta\gamma)}_{12(1,0,0)} d_1 + S^{(2\beta\gamma)}_{12(1,0,0)} d_2]^{(p,q,r)} = 0 \tag{49}$$

$$[S^{(1\beta\gamma)}_{13(1,0,0)} d_1 + S^{(2\beta\gamma)}_{13(1,0,0)} d_2]^{(p,q,r)} = 0. \tag{50}$$

We note that eqn (32a), which ensures continuity of tractions between adjacent cells in the periodic x_1 direction, is identically satisfied by the chosen displacement field representation owing to the periodic character of the composite material in this direction.

The equations that ensure traction continuity between individual subcells, as well as between individual cells, associated with the x_2 and x_3 directions, eqns (31b,c), and eqns (32b,c), are given by

$$[-12S^{(\alpha 1\gamma)}_{2j(0,1,0)} h_1 + S^{(\alpha 2\gamma)}_{2j(0,0,0)} - 6S^{(\alpha 2\gamma)}_{2j(0,1,0)} h_2]^{(p,q,r)} - [S^{(\alpha 2\gamma)}_{2j(0,0,0)} + 6S^{(\alpha 2\gamma)}_{2j(0,1,0)} h_2]^{(p,q-1,r)} = 0 \tag{51}$$

$$[-S^{(\alpha 1\gamma)}_{2j(0,0,0)} + \tfrac{1}{2} S^{(\alpha 2\gamma)}_{2j(0,0,0)} - 3S^{(\alpha 2\gamma)}_{2j(0,1,0)} h_2]^{(p,q,r)} + \tfrac{1}{2}[S^{(\alpha 2\gamma)}_{2j(0,0,0)} + 6S^{(\alpha 2\gamma)}_{2j(0,1,0)} h_2]^{(p,q-1,r)} = 0 \tag{52}$$

$$[-12S^{(\alpha\beta 1)}_{3j(0,0,1)} l_1 + S^{(\alpha\beta 2)}_{3j(0,0,0)} - 6S^{(\alpha\beta 2)}_{3j(0,0,1)} l_2]^{(p,q,r)} - [S^{(\alpha\beta 2)}_{3j(0,0,0)} + 6S^{(\alpha\beta 2)}_{3j(0,0,1)} l_2]^{(p,q,r-1)} = 0 \tag{53}$$

$$[-S^{(\alpha\beta 1)}_{3j(0,0,0)} + \tfrac{1}{2} S^{(\alpha\beta 2)}_{3j(0,0,0)} - 3S^{(\alpha\beta 2)}_{3j(0,0,1)} l_2]^{(p,q,r)} + \tfrac{1}{2}[S^{(\alpha\beta 2)}_{3j(0,0,0)} + 6S^{(\alpha\beta 2)}_{3j(0,0,1)} l_2]^{(p,q,r-1)} = 0 \tag{54}$$

where $j = 2$ and 3.

Equations (48)–(54) provide us with 44 additional relations among the zeroth-order and first-order stresses. These relations, together with eqn (47), can be expressed in terms of the unknown coefficients $W^{(\alpha\beta\gamma)}_{n(lmn)}$ by making use of eqns (39)–(46), providing a total of 60 of the required 104 equations necessary for the determination of these coefficients in the (p,q,r)th cell.

2.5.3. *Displacement continuity equations.* The additional 44 relations necessary to determine the unknown coefficients in the displacement field expansion are subsequently obtained by imposing displacement continuity conditions on an average basis at each subcell and cell interface. The continuity of displacements in the periodic x_1 direction at each subcell interface of the (p, q, r)th cell, eqn (33a), is satisfied by the following conditions:

$$[d_1 W^{(1\beta\gamma)}_{1(100)} + d_2 W^{(2\beta\gamma)}_{1(100)}]^{(p,q,r)} = 0 \tag{55}$$

$$[W^{(1\beta\gamma)}_{2(000)} + \tfrac{1}{4} d_1^2 W^{(1\beta\gamma)}_{2(200)} - W^{(2\beta\gamma)}_{2(000)} - \tfrac{1}{4} d_2^2 W^{(2\beta\gamma)}_{2(200)}]^{(p,q,r)} = 0 \tag{56}$$

$$[W^{(\alpha\beta 1)}_{3(000)} + \tfrac{1}{4}d_1^2 W^{(\alpha\beta 1)}_{3(200)} - W^{(\alpha\beta 2)}_{3(000)} - \tfrac{1}{4}d_2^2 W^{(\alpha\beta 2)}_{3(200)}]^{(p,q,r)} = 0. \tag{57}$$

The displacement continuity between neighboring cells in the periodic x_1 direction, eqn (34a), is automatically satisfied by the chosen displacement field representation which reflects the periodic character of the composite in this direction.

The displacement continuity conditions at the inner surfaces, eqns (33b,c), as well as between neighboring cells, eqns (34b,c), in the FG x_2 and x_3 directions, yield

$$[W^{(\alpha 1\gamma)}_{2(000)} + \tfrac{1}{2}h_1 W^{(\alpha 1\gamma)}_{2(010)} + \tfrac{1}{4}h_1^2 W^{(\alpha 1\gamma)}_{2(020)} - W^{(\alpha 2\gamma)}_{2(000)} + \tfrac{1}{2}h_2 W^{(\alpha 2\gamma)}_{2(010)} - \tfrac{1}{4}h_2^2 W^{(\alpha 2\gamma)}_{2(020)}]^{(p,q,r)} = 0 \tag{58}$$

$$[W^{(\alpha 2\gamma)}_{2(000)} + \tfrac{1}{2}h_2 W^{(\alpha 2\gamma)}_{2(010)} + \tfrac{1}{4}h_2^2 W^{(\alpha 2\gamma)}_{2(020)}]^{(p,q+1,r)} = [W^{(\alpha 1\gamma)}_{2(000)} - \tfrac{1}{2}h_1 W^{(\alpha 1\gamma)}_{2(010)} + \tfrac{1}{4}h_1^2 W^{(\alpha 1\gamma)}_{2(020)}]^{(p,q+1,r)} \tag{59}$$

$$[W^{(\alpha 1\gamma)}_{3(000)} + \tfrac{1}{2}h_1 W^{(\alpha 1\gamma)}_{3(010)} + \tfrac{1}{4}h_1^2 W^{(\alpha 1\gamma)}_{3(020)} - W^{(\alpha 2\gamma)}_{3(000)} + \tfrac{1}{2}h_2 W^{(\alpha 2\gamma)}_{3(010)} - \tfrac{1}{4}h_2^2 W^{(\alpha 2\gamma)}_{3(020)}]^{(p,q,r)} = 0 \tag{60}$$

$$[W^{(\alpha 2\gamma)}_{3(000)} + \tfrac{1}{2}h_2 W^{(\alpha 2\gamma)}_{3(010)} + \tfrac{1}{4}h_2^2 W^{(\alpha 2\gamma)}_{3(020)}]^{(p,q+1,r)} = [W^{(\alpha 1\gamma)}_{3(000)} - \tfrac{1}{2}h_1 W^{(\alpha 1\gamma)}_{3(010)} + \tfrac{1}{4}h_1^2 W^{(\alpha 1\gamma)}_{3(020)}]^{(p,q+1,r)} \tag{61}$$

$$[W^{(\alpha\beta 1)}_{2(000)} + \tfrac{1}{2}l_1 W^{(\alpha\beta 1)}_{2(001)} + \tfrac{1}{4}l_1^2 W^{(\alpha\beta 1)}_{2(002)} - W^{(\alpha\beta 2)}_{2(000)} + \tfrac{1}{2}l_2 W^{(\alpha\beta 2)}_{2(001)} - \tfrac{1}{4}l_2^2 W^{(\alpha\beta 2)}_{2(002)}]^{(p,q,r)} = 0 \tag{62}$$

$$[W^{(\alpha\beta 2)}_{2(000)} + \tfrac{1}{2}l_2 W^{(\alpha\beta 2)}_{2(001)} + \tfrac{1}{4}l_2^2 W^{(\alpha\beta 2)}_{2(002)}]^{(p,q,r)} = [W^{(\alpha\beta 1)}_{2(000)} - \tfrac{1}{2}l_1 W^{(\alpha\beta 1)}_{2(001)} + \tfrac{1}{4}l_1^2 W^{(\alpha\beta 1)}_{2(002)}]^{(p,q,r+1)} \tag{63}$$

$$[W^{(\alpha\beta 1)}_{3(000)} + \tfrac{1}{2}l_1 W^{(\alpha\beta 1)}_{3(001)} + \tfrac{1}{4}l_1^2 W^{(\alpha\beta 1)}_{3(002)} - W^{(\alpha\beta 2)}_{3(000)} + \tfrac{1}{2}l_2 W^{(\alpha\beta 2)}_{3(001)} - \tfrac{1}{4}l_2^2 W^{(\alpha\beta 2)}_{3(002)}]^{(p,q,r)} = 0 \tag{64}$$

$$[W^{(\alpha\beta 2)}_{3(000)} + \tfrac{1}{2}l_2 W^{(\alpha\beta 2)}_{3(001)} + \tfrac{1}{4}l_2^2 W^{(\alpha\beta 2)}_{3(002)}]^{(p,q,r)} = [W^{(\alpha\beta 1)}_{3(000)} - \tfrac{1}{2}l_1 W^{(\alpha\beta 1)}_{3(001)} + \tfrac{1}{4}l_1^2 W^{(\alpha\beta 1)}_{3(002)}]^{(p,q,r+1)}. \tag{65}$$

Equations (55)–(65) comprise the required additional 44 relations.

2.5.4. *Governing equations for the unknown coefficients in the displacement expansion.* The equilibrium equations, eqn (47), together with the traction and displacement continuity equations, eqns (48)–(54) and (55)–(65), respectively, altogether form 104 equations in the 104 unknowns $W^{(\alpha\beta\gamma)}_{i(lmn)}$ which govern the equilibrium of a subcell $(\alpha\beta\gamma)$ within the (p,q,r)th cell in the interior. As in the thermal problem, a different treatment must be adopted for the boundary cells $(p,1,r)$, (p,N_q,r), and $(p,q,1)$ and (p,q,N_r). For $(p,1,r)$, the above relations are operative, except eqns (51) and (52), which follow from the continuity of tractions between a given cell and the preceding one. These eight equations must be replaced by the conditions of continuity of tractions at the interior interfaces of the cell $(p,1,r)$ and by the applied tractions at $x_1 = 0$, eqn (35a). For the cell (p,N_q,r), the previously derived governing equations are operative except for the four relations given by eqns (59) and (61) which are obviously not applicable. These are replaced by the imposed traction conditions at the surface $x_2 = H$, eqn (35b). Similar arguments hold for boundary cells $(p,q,1)$ and (p,q,N_r). Consequently, the governing equations at both interior and boundary cells form a system of $104N_qN_r$ linear algebraic equations in the field variables within the cells of the functionally graded composite. The final form of this system of equations is symbolically represented below

$$\mathbf{KU} = \mathbf{f}. \tag{66}$$

where the structural stiffness matrix $\mathbf{K}$ contains information on the geometry and thermomechanical properties of the individual subcells $(\alpha\beta\gamma)$ within the cells comprising the functionally graded composite, the displacement coefficient vector $\mathbf{U}$ contains the unknown coefficients that describe the displacement field in each subcell, i.e. $\mathbf{U} = [\mathbf{U}^{(111)}_{(lmn)}, \ldots, \mathbf{U}^{(222)}_{(lmn)}]$ where $\mathbf{U}^{(\alpha\beta\gamma)}_{(lmn)} = [W_{1(lmn)}, \ldots, W_{3(002)}]^{(\alpha\beta\gamma)}$, and the mechanical force vector $\mathbf{f}$ contains information on the boundary conditions and the thermal loading effects generated by the applied temperature.

2.5.5. *Extension to generalized plane strain in the* x_1 *direction.* As indicated previously, the present formulation in which the displacement components within the subcell $(\alpha\beta\gamma)$ of the (p,q,r)th cell are expanded in accordance with eqn (37) leads to the result that the strain $\varepsilon_{11}^{(\alpha\beta\gamma)}$ averaged over the entire volume $V = (d_1+d_2)HL$ occupied by the functionally graded composite is zero.

$$\bar{\varepsilon}_{11} = \frac{1}{V}\sum_{q=1}^{N_2}\sum_{r=1}^{N_3}\sum_{\alpha,\beta,\gamma=1}^{2} v_{(\alpha\beta\gamma)}^{(pqr)}\varepsilon_{11}^{(\alpha\beta\gamma)} = 0. \tag{67}$$

It is frequently desirable to obtain a generalized plane strain situation where $\bar{\varepsilon}_{11}$ = non-zero constant. This can be achieved by adding a constant term to the first equation in (37) and applying a homogenization procedure in the x_1 periodic direction. It can be shown that the only equation affected by this process is eqn (55) which must be replaced by (Aboudi *et al.*, 1995):

$$[d_1 W_{1;100}^{(\alpha\beta\gamma)} + d_2 W_{1;100}^{(2\beta\gamma)}]^{(p,q,r)} = (d_1+d_2)\bar{\varepsilon}_{11}, \tag{68}$$

where $\bar{\varepsilon}_{11}$ is an unknown value that must be determined from the condition that $\bar{\sigma}_{11} = 0$, where $\bar{\sigma}_{11}$ is the average of $\sigma_{11}^{(\alpha\beta\gamma)}$ over the entire volume of the composite:

$$\bar{\sigma}_{11} = \frac{1}{V}\sum_{q=1}^{N_2}\sum_{r=1}^{N_3}\sum_{\alpha,\beta,\gamma=1}^{2} v_{(\alpha\beta\gamma)}^{(pqr)}\sigma_{11}^{(\alpha\beta\gamma)} = 0. \tag{69}$$

3. APPLICATIONS

The approach outlined in the foregoing is employed to investigate the response of a symmetrically laminated B/Ep–Ti plate subjected to a uniform temperature change of -154.45 C. This temperature change simulates cool down from the fabrication temperature which induces residual stresses into the individual plies owing to a thermal expansion mismatch between the boron/epoxy and the titanium plies. The residual stress fields exhibit large gradients near the free edges of the laminate which were investigated by Herakovich (1976) using the finite-element approach. Herein, we first compare the finite-element results for the stress fields near the free edge with the predictions of HOTFGM-2D, treating the boron/epoxy (B/Ep) plies as homogeneous with equivalent effective (or homogenized) properties. This comparison demonstrates the capability of the new coupled theory to capture large gradients in the stress fields at geometric and material discontinuities (i.e. along interfaces at the free edge of a laminated plate) in the presence of a spatially uniform temperature field. Subsequently, the effect of microstructure of the B/Ep plies on the free-edge fields is investigated in view of the large diameter of the boron fibers and relatively small thickness of the B/Ep plies. Finally, the utility of nonuniformly distributing (i.e. functionally grading) boron fibers in the B/Ep plies near the free edge to reduce the large stress gradients in this region is demonstrated.

The cross-section geometry of the investigated laminate is given in Fig. 3. The thickness, designated by H in the figure, and the width L produce a laminate with an aspect ratio of $L/H = 12.5$. The direction of the boron fibers in the external B/Ep plies is parallel to the x_1 (out-of-plane) axis, along which the laminate is considered to be infinitely long. The volume fraction of the fibers is 0.50. The resulting macroscopic thermo-mechanical properties of the B/Ep plies and the titanium inner sheets are given in Table 1. As in Herakovich (1976), these properties are considered to be temperature-independent. Comparison of the thermal expansion coefficients of the B/Ep plies and the titanium sheets reveals a significant mismatch in the transverse direction (along the x_3 axis), with a smaller mismatch in the out-of-plane direction. Figure 4 illustrates the axial and transverse thermal expansion coefficients, α_A^* and α_T^*, respectively, of the B/Ep ply as a function of the fiber content v_f generated using the method of cells micromechanics model (Aboudi, 1991). Included in the

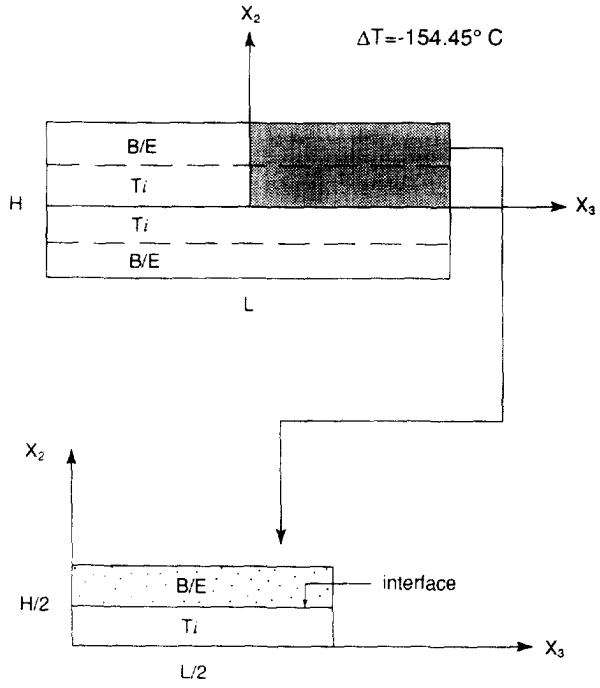

Fig. 3. Cross-section of a [B Ep-Ti]$_s$ laminate.

Table 1. Material properties of the boron epoxy plies ($\nu_A^* = 0.50$) and titanium sheets

Material	E_A^* (GPa)	E_T^* (GPa)	ν_A^*	α_A^* (10^{-6} C^{-1})	α_T^* (10^{-6} C^{-1})
B/Ep	206.8	18.6	0.21	4.5	30.6
Ti	118.6	118.6	0.34	8.5	8.5

Subscripts A and T denote axial and transverse quantities, respectively.

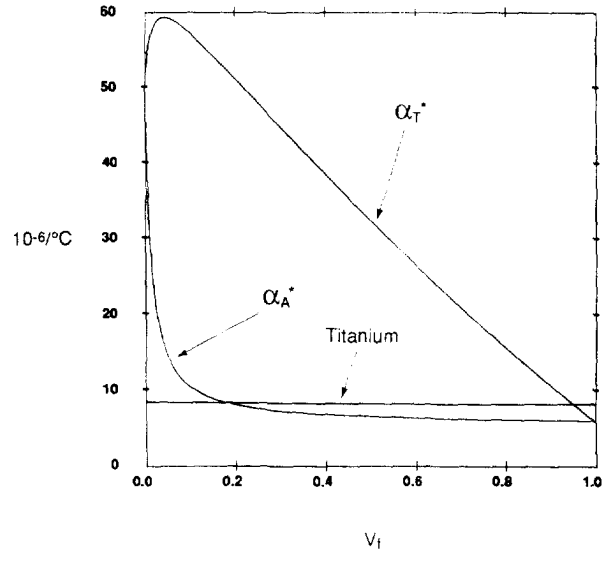

Fig. 4. Effective normal and transverse thermal expansion coefficients of B/Ep as a function of the fiber volume fraction. Also shown in the figure is the CTE of the isotropic titanium sheet.

Table 2. Material properties of boron fiber and epoxy matrix

Material	E (GPa)	ν	α (10^{-6} C^{-1})
Boron fiber	417.0	0.13	6.0
Epoxy matrix	5.24	0.35	50.0

E and ν denote the Young's modulus and Poisson's ratio, respectively, and α is the coefficient of thermal expansion.

figure is the thermal expansion coefficient of the isotropic titanium sheet. The thermoelastic properties of the boron fibers and the epoxy matrix used to generate this figure are given in Table 2. The graphical results shown in Fig. 4 indicate that the large thermal expansion mismatch between the B/Ep and the Ti plies in the transverse direction (i.e. x_3) can be reduced by increasing the fiber content of the B/Ep ply above the current value of 0.50. It is expected that the reduction of the transverse CTE mismatch will lead to a decrease in the transverse residual stresses and thus the severity of the free-edge stress gradients. Figure 4 thus provides a motivation for using functionally graded fiber architectures in the vicinity of the free edge to decrease the transverse thermal expansion mismatch in this region, and thus reduce the interlaminar stresses. Since the interlaminar stress field is a localized effect, it is reasonable to expect that it is sufficient to limit grading of the fiber content in the B/Ep plies to the immediate vicinity of the free edge.

3.1. *Comparison of HOTFGM-2D and FE predictions based on homogenized B/Ep properties*

Figure 5 presents comparison of the normal (σ_{11}, σ_{22}, σ_{33}) and shear (σ_{23}) stress distributions in the titanium sheet along the interface separating the B/Ep and Ti plies (see Fig. 3) generated using HOTFGM-2D and the finite-element analysis of Herakovich (1976). These results were obtained using the effective or homogenized thermo-mechanical properties of the B/Ep and Ti plies given in Table 1. As stated previously, the illustrated stress distributions were induced by subjecting the [B/Ep-Ti]$_5$ laminate to a uniform temperature change of -154.45 C. Since the interfacial traction continuity conditions are imposed in an average sense in HOTFGM-2D, the stress components which are tractions along an interface are averaged as well. Hence the stress components σ_{22} and σ_{23} in a given subcell $(\alpha\beta\gamma)$ of the cell (p, q, r) obtained from the higher-order theory were calculated as follows:

$$\sigma_{2j} = \frac{1}{d_\alpha l_\beta^{(r)}} \int_{x_2^{(\alpha-1)}}^{x_2^{(\alpha)}} \int_{x_3^{(\beta-1)}}^{x_3^{(\beta)}} \sigma_{2j}^{(\alpha\beta\gamma)} \, \mathrm{d}\bar{x}_3^{(\beta)} \, \mathrm{d}\bar{x}_1^{(\alpha)}, \quad j = 2, 3.$$

The stress components $\sigma_{11}^{(\alpha\beta\gamma)}$ and $\sigma_{33}^{(\alpha\beta\gamma)}$, on the other hand, were not averaged.

The finite-element results were generated using three different meshes, indicated by B-1, B-2 and B-3 in the figure, with each successive mesh undergoing increasingly greater refinement until satisfactory convergence was obtained. Due to the symmetry of the considered plate with respect to the x_2 and x_3 axes, only one quarter of the plate needs to be analysed (see Fig. 3) under appropriate boundary conditions which reflect these symmetries. The higher-order theory results were generated by discretizing the quarter-plate in the manner shown in Fig. 6. The level of discretization at the free edge shown in this figure was determined by performing a convergence study in which increasingly greater number of subcells was introduced into the region immediately adjacent to the free edge, defined by $0.49L \leqslant x_3 \leqslant 0.5L$ (see Fig. 6), starting with two subcells and ending with 100 subcells. Figure 7 illustrates the relatively rapid convergence of the maximum normal stresses σ_{22} and σ_{11} (in the titanium ply) along the interface at the free edge with increasing number of free-edge subcells. Similar results were obtained for the remaining stress components, thereby justifying the employed level of discretization shown in Fig. 6.

The stress profiles presented in Fig. 5 exhibit large stress gradients in the immediate vicinity of the free edge. Away from the free edge, these stress distributions attain uniform values that can be predicted using the classical lamination theory for sufficiently large L/H

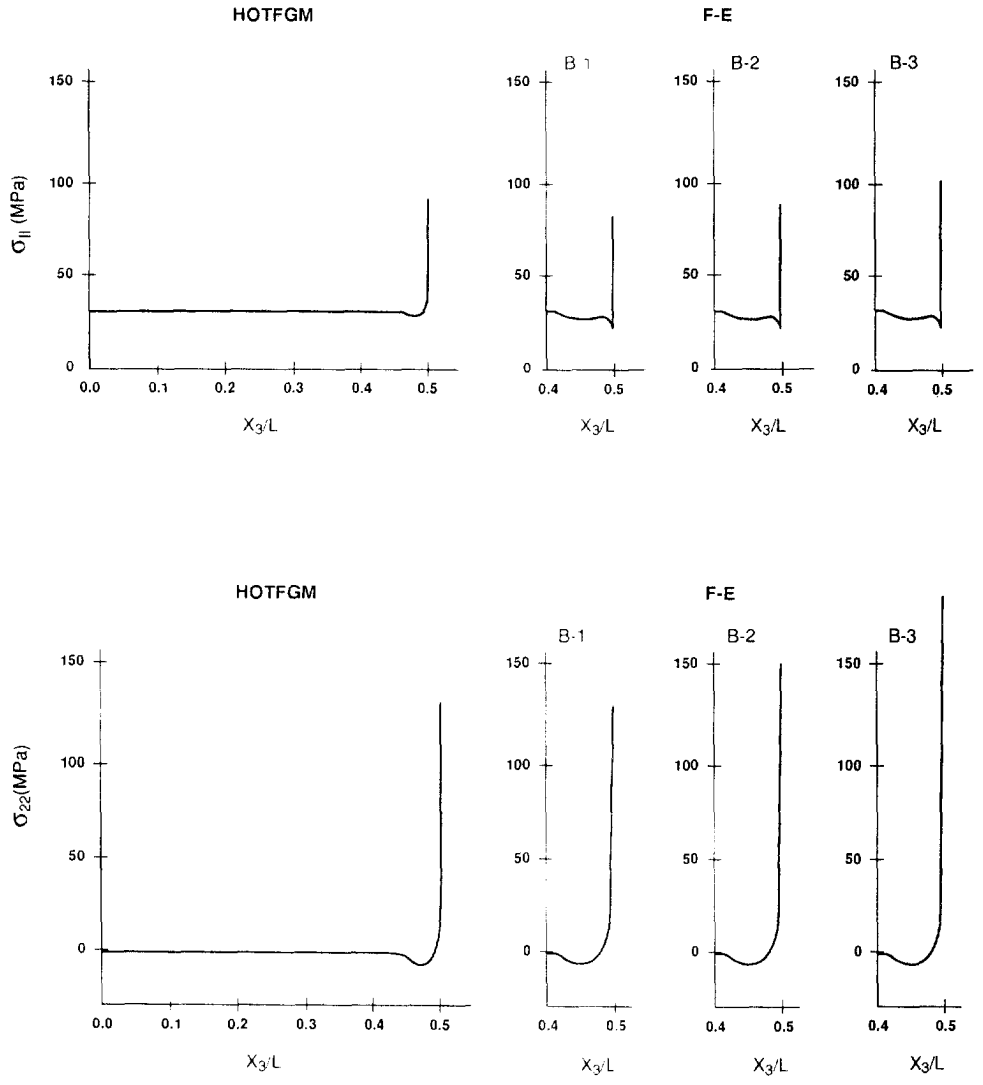

Fig. 5. Normal and shear stress distributions in the titanium ply at the interface separating B-Ep and Ti plies due to a temperature change of $\Delta T = -154.45$ °C. Comparison between the predictions of HOTFGM-2D and F-E analysis.

aspect ratios. The rapid decay of the interlaminar stresses to their lamination theory or far-field values occurs over a distance that is approximately one laminate thickness H from the free edge. The far-field values of the normal stresses σ_{11}, σ_{22} and σ_{33} predicted by the coupled higher-order theory are 29.9, 0.0, and -54.95 MPa, respectively. The far-field value of the shear stress σ_{23} is 0.0. These results coincide with the lamination theory predictions.

In the vicinity of the free-edge, the large gradient and magnitude of the σ_{11} stress component obtained from the coupled higher-order analysis compares very favorably with the finite-element results generated with the most refined mesh. The behavior of the σ_{22} stress component near the free edge predicted by the higher-order theory also compares favorably with the finite-element results, lying between the B-1 and B-3 mesh predictions. This component is often responsible for delamination initiation at the free edge when it is tensile, as is the present situation. The normal stress component σ_{33} is in the direction of the free edge and thus has to vanish on the lateral surface $x_3/L = 0.5$. Both the higher-order theory and finite-element predictions indicate that this stress component does tend to zero with decreasing distance from the edge. The finite-element results indicate an initial decrease in this stress component relative to the far-field value (i.e. an increase in the magnitude of the compressive stress) followed by rapid reversal and decay to zero. The magnitude of this initial decrease predicted by the HOTFGM-2D analysis, however, is substantially smaller

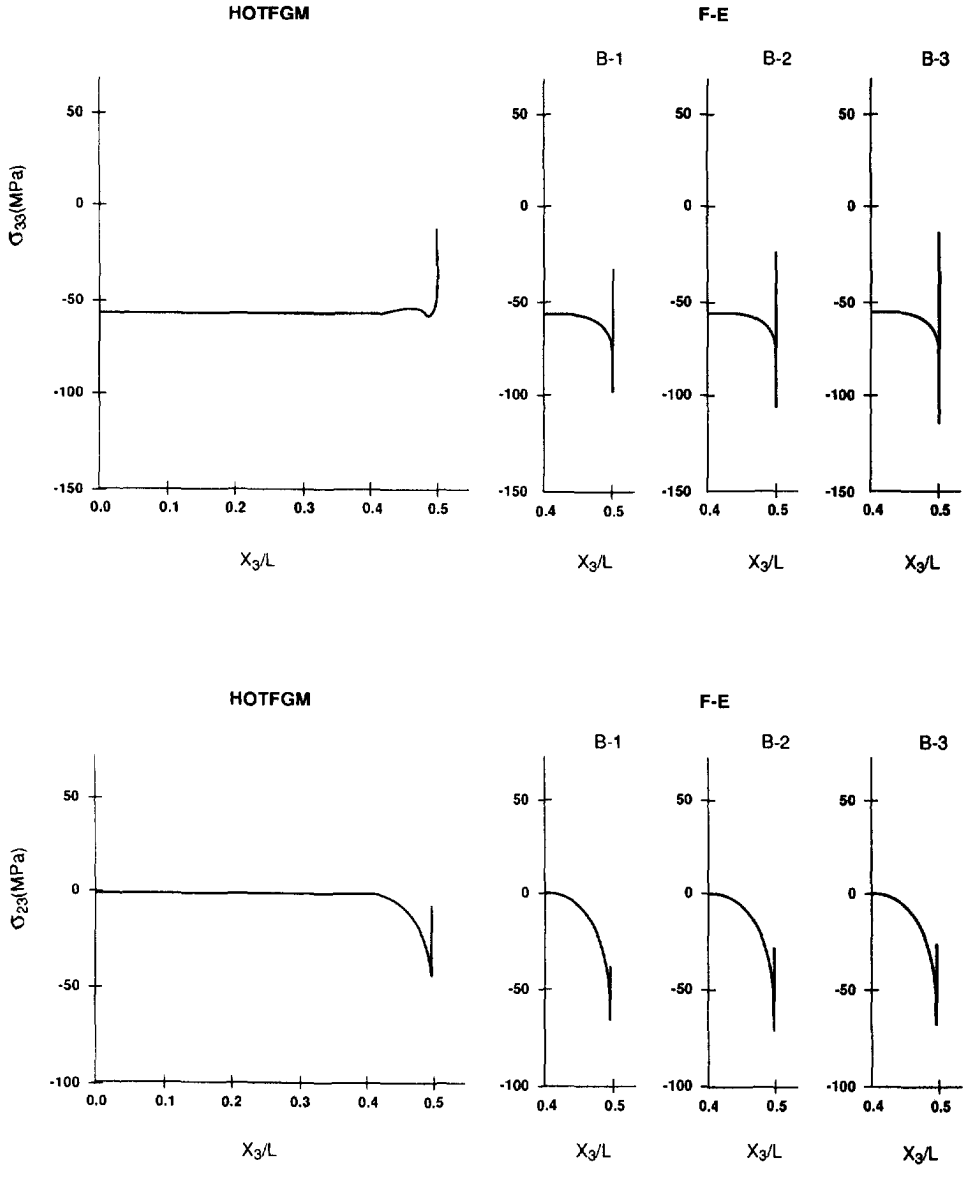

Fig. 5 (*continued*)

relative to the finite-element predictions. On the other hand, the magnitude of the normal stress σ_{33} in the immediate vicinity of the free edge is closer to zero than that predicted by the finite-element analysis using the most refined mesh (B-3). Finally, the comparison of the shear stress components σ_{23} predicted by the two approaches is also favorable. This stress component also undergoes a rapid reversal at the free edge, initially decreasing (i.e. increasing in magnitude), then reversing direction and rapidly decaying to zero. The magnitude of the maximum shear stress at the reversal point predicted by the coupled higher-order theory is somewhat smaller than that predicted by the finite-element analysis. On the other hand, the shear stress at the free edge predicted by HOTFGM-2D is much smaller (in fact almost zero) than that predicted by the finite-element approach.

The comparison of the stresses in the titanium sheet at the B/Ep-Ti interface generated using the HOTFGM-2D and finite-element approaches indicates that the major features of the near free-edge stress fields are correctly captured by the coupled higher-order theory. While in some instances the actual magnitudes are not in perfect agreement, it is not clear at this point whether the problem lies with the HOTFGM-2D or finite-element results since the discrepancies, when they occur, are not sufficiently consistent to point to either of the

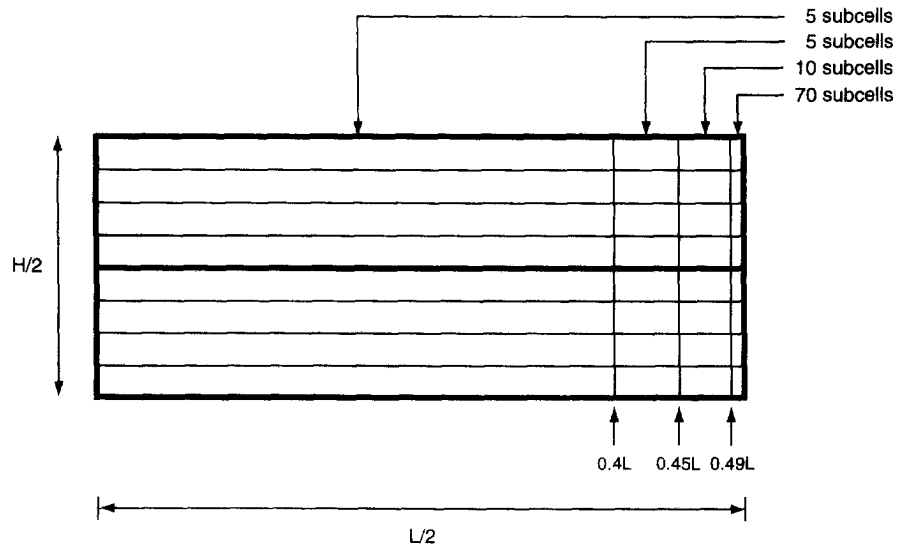

Fig. 6. Quarter-plate volume discretization used to generate the HOTFGM-2D results.

two approaches as a potential culprit. It is clear, however, based on the presented comparison, that the coupled higher-order theory is sufficiently sensitive to capture the large stress gradients, and even rapid stress reversals (see σ_{23} distribution in Fig. 5) that occur in regions of geometric discontinuities such as the free edge. It is also reassuring that convergent results can be obtained with a sufficient level of volume discretization. This sets the stage for investigating the effect of microstructure on the free-edge stress fields (using the quarter-plate discretization shown in Fig. 6).

3.2. *Effect of microstructure of the B/Ep plies on the free-edge stress fields*

The results presented heretofore have been generated by treating the B/Ep plies as homogeneous with certain effective or homogenized thermo-mechanical properties. These

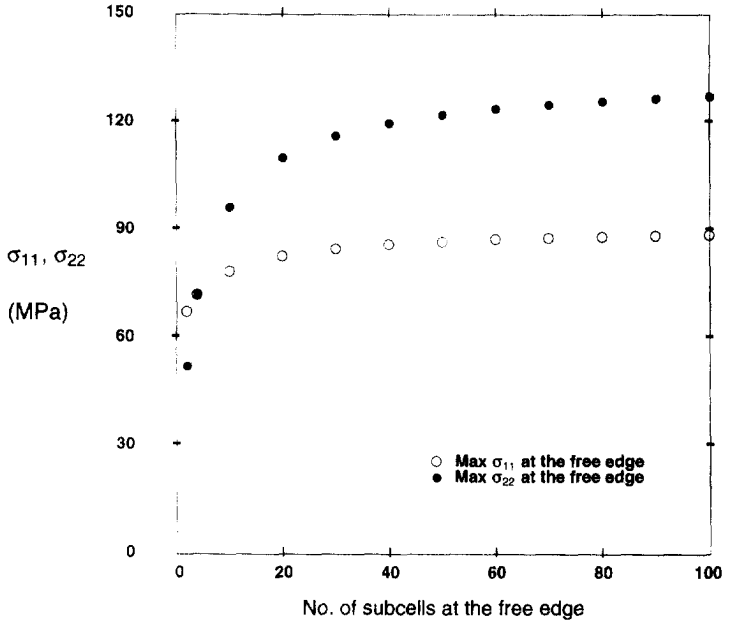

Fig. 7. Convergence behavior of the maximum normal stresses σ_{22} and σ_{11} (in the titanium ply) at the B/Ep-Ti interface in the subcell next to the free edge as a function of the number of subcells in the free-edge region $0.49L \leqslant x_1 \leqslant 0.5L$.

properties can be either measured directly in the laboratory or determined using a micromechanics scheme when macroscopically homogeneous deformation fields are imposed. However, when the reinforcement size (i.e. fiber diameter) is large relative to the thickness of a composite ply, which is the case with boron-reinforced and silicon carbide-reinforced composites, the meaning of material property becomes fuzzy in the presence of large stress gradients as previously discussed. This is the case in the present situation at the free edge given the large boron fiber diameter relative to the thickness of the B/Ep ply. It is thus important to characterize the error introduced in the analysis of free-edge stress fields based on the homogenized properties of the B/Ep ply.

Figure 8 illustrates eight configurations of the $[B/Ep\text{-}Ti]_s$ laminate with increasingly refined microstructure of the B/Ep plies at the free edge that were investigated in order to determine the effect of the microstructure on the stress fields. The overall dimensions of the laminate and the individual plies are the same as in the previous problem with homogenized B/Ep properties. The number of boron fibers in the through-thickness direction of the B/Ep plies was taken as two, and the fiber dimensions were chosen to yield the same fiber volume fraction of 0.50 as in the previous problem. The properties of the boron fiber and epoxy matrix reported in Table 2 produce the same homogenized properties for the B/Ep plies as those employed previously. These properties were assigned to the fiber and matrix phases in the regions of the B/Ep plies shown in Fig. 8 with increasingly refined microstructures. Outside of those regions, homogenized thermo-mechanical properties were employed for the B/Ep plies.

Figure 9 presents the normal stress σ_{22} in the titanium sheet at the B/Ep-Ti interface for the eight configurations shown in Fig. 8. This stress component, due to its tensile

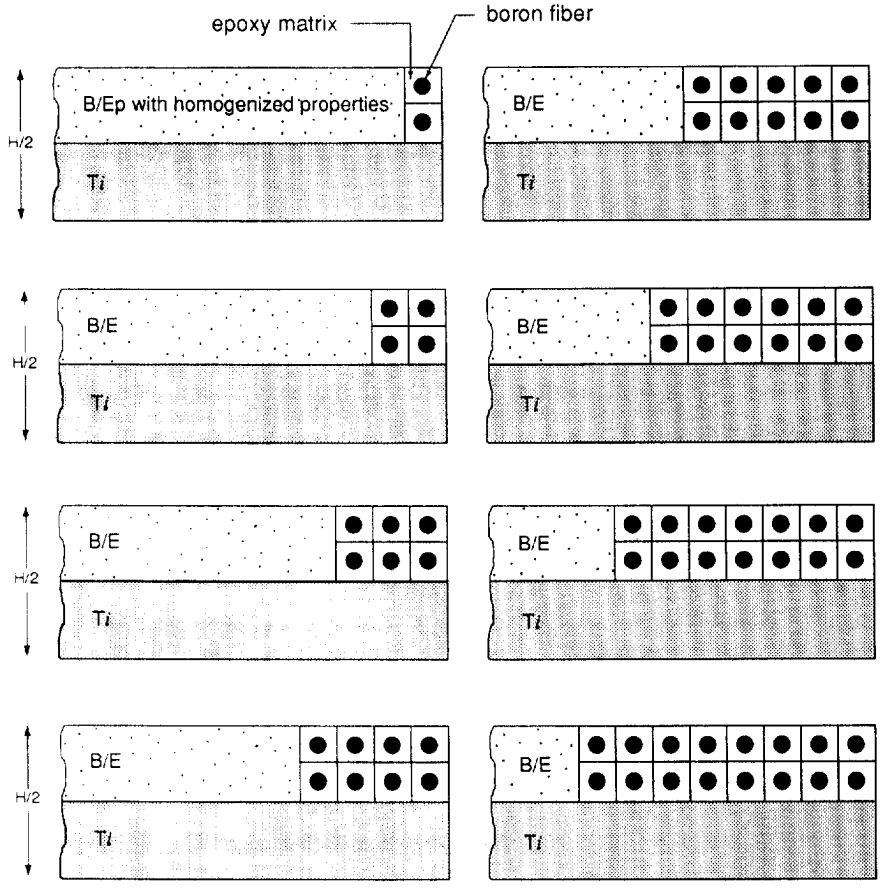

Fig. 8. Schematic of eight configurations of the [B Ep-Ti]$_s$ laminate showing increasingly refined microstructure at the free edge.

character, is responsible for the initiation of delamination, and thus is of particular importance for the considered configuration subjected to the given thermal load. Examination of the individual figures for each configuration reveals an increasingly complex character of the stress distribution near the free edge with increasing refinement of the microstructure that is due to the interaction with the individual boron fibers in the adjacent B/Ep ply. The stress distributions are characterized by rapid oscillations that coincide with the locations of the boron fibers in the B/Ep plies directly above the titanium sheet. The reversals in the sign of the stress oscillations could potentially have an effect on the delamination process. More importantly, however, the maximum normal stress at the free edge increases with increasing refinement of the microstructure. This is clearly illustrated in Fig. 10 where the

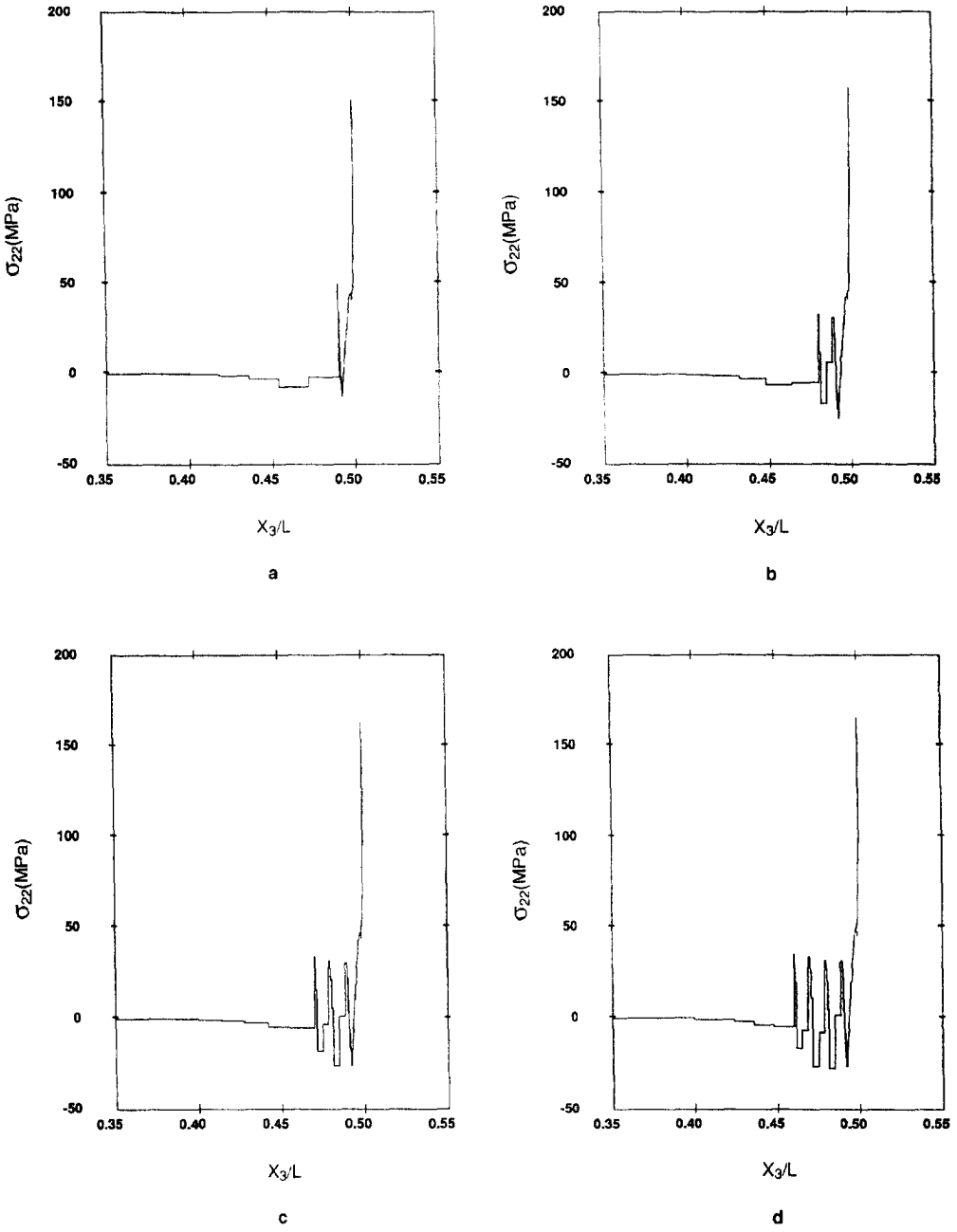

Fig. 9. Normal stress σ_{22} distributions in the titanium ply at the interface separating B/Ep and Ti plies due to a temperature change of $\Delta T = -154.45$ C for the eight configurations of Fig. 8.

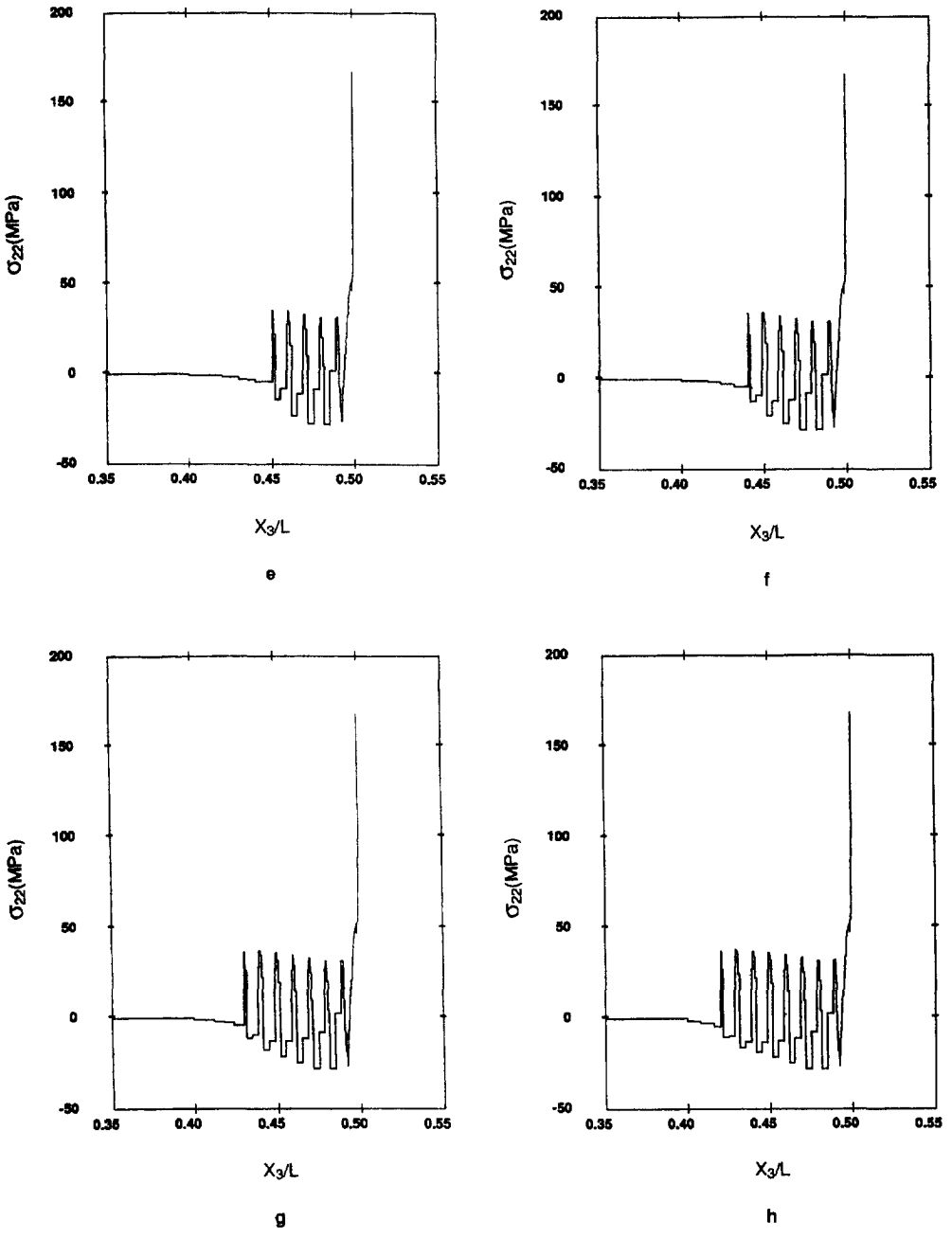

Fig. 9 (*continued*)

maximum stress σ_{22} at the free edge for the eight different configurations has been normalized by the corresponding stress obtained from the HOTFGM-2D analysis using homogenized B/Ep properties. As is observed, the actual maximum stress at the free edge in the presence of microstructure asymptotically approaches a uniform value with increasing number of fiber/matrix cells in the B/Ep ply at the free edge. At least seven cells are required in the horizontal direction at the free edge to capture the actual maximum value of σ_{22} in the titanium ply. More importantly, the actual maximum stress is 35% greater than the corresponding stress obtained using homogenized properties of the B/Ep plies. This is a significant difference that cannot be overlooked in predicting the onset of delamination, revealing the shortcoming of the homogenized continuum approach in the presence of course microstructure and large stress gradients.

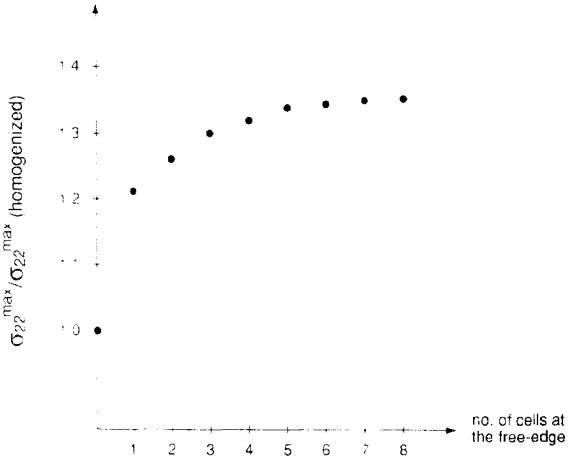

Fig. 10. Normalized maximum stress σ_{22} in the titanium ply at the free-edge of the laminate at the interface separating B Ep and Ti plies owing to a temperature change of $\Delta T = -154.45$ C as a function of the refined microstructure for the eight configurations of Fig. 8. The normalization is performed with respect to the corresponding maximum stress obtained from the analysis based on homogenized B Ep properties

3.3. *Delamination control through microstructural tailoring of the B Ep plies*

As illustrated in the preceding sections, the large thermally induced interlaminar stresses in the vicinity of the free edge, and in particular the large tensile normal σ_{22} stress commonly called *peel stress*, may be sufficiently large to initiate delamination during fabrication cool down or subsequent mechanical loading. It is of technological interest to reduce this stress component in order to increase the load-bearing capability of such laminates. In this section we investigate the possibility of accomplishing this through the use of functionally graded architectures in the B Ep plies.

We choose two approaches to reduce the peel stress at the free edge. In the first approach, we selectively remove fibers from the B Ep plies in the vicinity of the free edge in order to create a local clamping in the vertical direction at the lateral surface of the laminate. It is presumed that this localized clamping arises from the tendency of the matrix phase to contract more than the surrounding B Ep material under the given temperature change, and that the contraction in the vertical direction has a greater effect on the stress field than the contraction in the horizontal direction. Since eight fiber/matrix cells in the B/Ep plies at the free edge are sufficient to capture the actual stress field in the presence of microstructural details (see Fig. 10), we use this configuration to test the hypothesis described above. Figure 11 presents the interlaminar peel stress profiles generated by removing one and two columns of fibers in the vicinity of the free edge. Figure 11a illustrates the interlaminar peel stress distribution for the baseline eight-cell configuration with no columns of fibers removed, while Fig. 11b–d presents the corresponding distributions for the configurations with column 2, columns 3 and 4, and columns 2 and 3 removed. The results indicate that the removal of the columns of fibers generally tends to lower the normal peel stress in the regions directly below the missing fibers. Furthermore, the magnitude of the compressive stress in the cells adjacent to the free edge is also increased. However, the maximum tensile stress at the free edge itself is actually increased when the fibers are removed. This is illustrated in Fig. 12 which presents the maximum free-edge peel stress in the configurations with the missing fibers normalized with respect to the corresponding value of the baseline configuration given in Fig. 11a. The greatest increase in the maximum value of the free-edge peel stress occurs in the configuration with the columns 2 and 3 removed, while the smallest increase occurs in the configuration with the columns 3 and 4 removed. Thus it appears that the increased tendency of the matrix with the missing fibers to contract in the vertical direction is more than offset by the horizontal contraction tendency. The overall effect is to increase the thermal expansion mismatch between B/Ep and Ti plies in the horizontal direction, resulting in the increase of the maximum peel stress at the free edge.

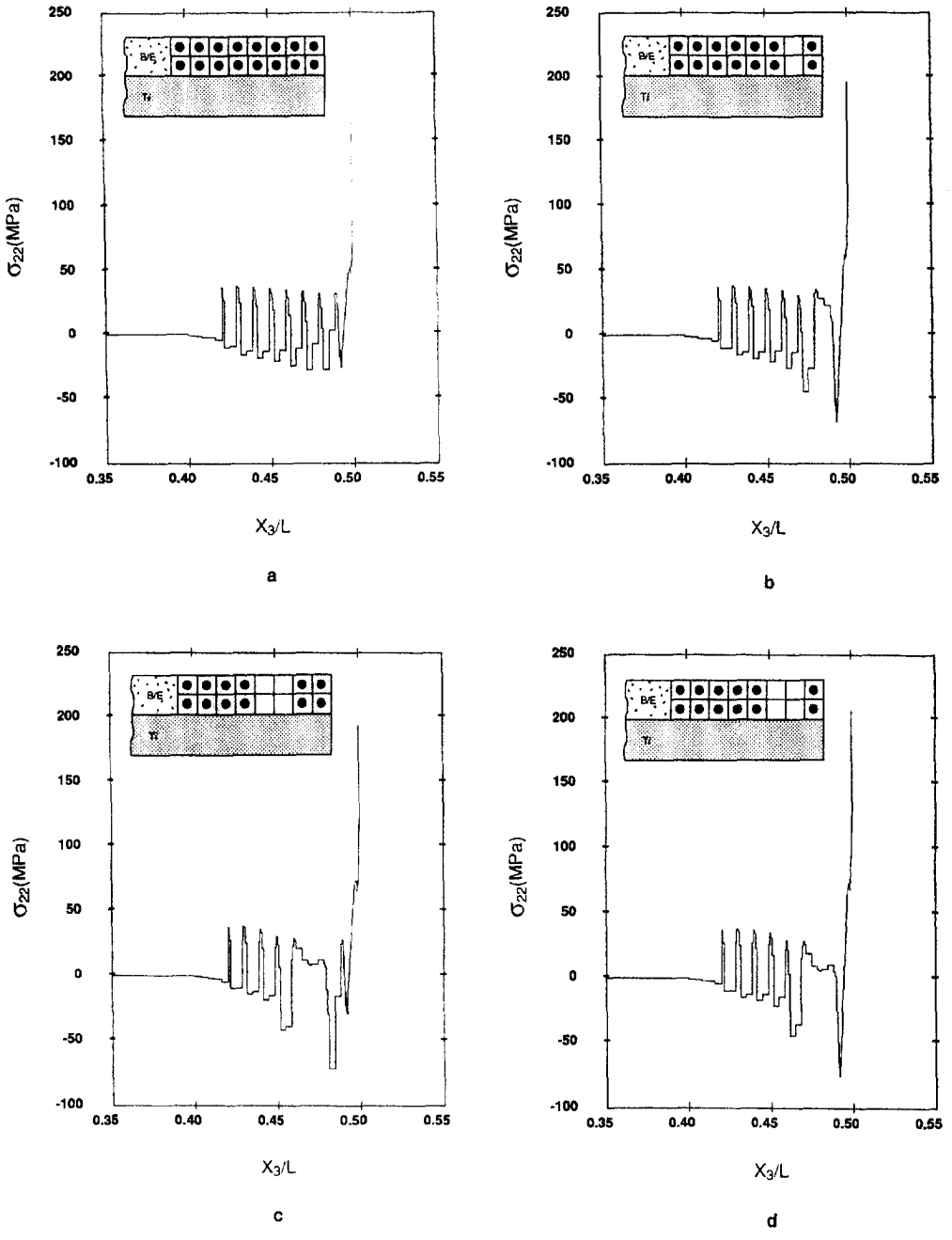

Fig. 11. Effect of removing fibers near the free-edge of the laminate on the normal stress σ_{22} distribution in the titanium ply at the interface separating B/Ep and Ti plies owing to a temperature change of $\Delta T = -154.45$ C.

The above exercise also sheds light on the effect of imperfections in fiber spacing near the free edge that may arise due to poor fiber placement control during fabrication. The results suggest that a localized increase in the thermal expansion mismatch between adjacent plies caused by missing fibers near the free edge will have a detrimental effect on the laminate's delamination resistance.

In the second approach used to reduce the interlaminar peel stress at the free edge, the fiber spacing in the horizontal direction was decreased in a linear manner with decreasing distance from the free edge. This effectively increases the local fiber volume fraction in the B/Ep plies which, in turn, decreases the transverse thermal expansion mismatch between

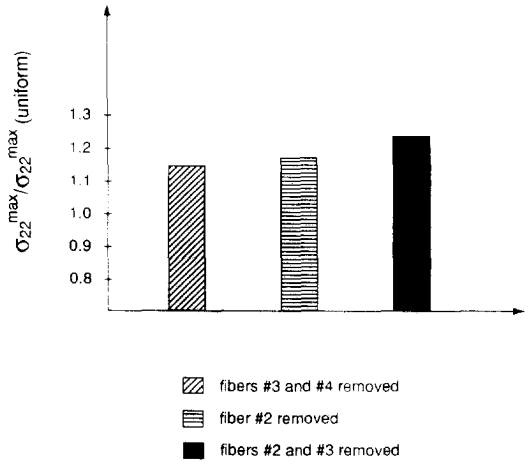

Fig. 12. Maximum stress σ_{22} in the titanium ply at the free-edge of the laminate at the interface separating B Ep and Ti plies due to a temperature change of $\Delta T = -154.45$ C obtained from distributions of Fig. 11, normalized with respect to the corresponding maximum stress obtained from the configuration with uniformly spaced fibers.

the adjacent plies at the free edge as is observed in Fig. 4. The results presented in Figs 11 and 12 indeed indicate that the local fiber volume fraction has a significant effect on the interlaminar stresses at the free edge, thereby supporting this second approach in reducing the peel stress. In addition to decreasing the horizontal fiber spacing in the vicinity of the free edge, the two rows of fibers were also shifted vertically in a uniform manner in order to bring them closer to the B/Ep–Ti interface and thus decrease the local thermal expansion mismatch in the thickness direction.

The functional grading of the fiber distribution in the horizontal direction was accomplished as follows. The total horizontal distance occupied by the eight fiber cells was 2032 μm. The distance of the center of the first fiber from the free edge was taken to be 97.36 μm. This was chosen such that the distance between the eighth fiber and the homogenized B/Ep material was 215.9 μm. This is exactly one half of the width of the unit cell with a fiber volume fraction of 0.50 in the uniformly spaced configuration. The distances between the centers of the eight fibers were linearly increased with increasing distance from the free edge in the manner illustrated in Table 3.

Figure 13 presents the four different fiber architectures near the free edge in the B/Ep plies that were generated using the combination of horizontal and vertical shifting of the boron fibers. The relative locations of the fibers with respect to the dimensions of the B/Ep plies are the same as in the actual configurations. The baseline configuration is the uniformly spaced configuration considered previously with center-to-center fiber spacing of 254.0 μm, shifted horizontally towards the free edge such that the location of the center of the first fiber coincides with the center of the first fiber in the linearly spaced configuration (i.e. 97.36 μm from the free edge). The second configuration was generated from the first by

Table 3. Center-to-center distances between fibers in the cells at the free edge in the linearly spaced configurations

Adjacent fibers from the free edge	Center-to-center distance between adjacent fibers (μm)
Free edge 1	97.36
1 2	201.08
2 3	215.90
3 4	230.70
4 5	245.50
5 6	260.35
6 7	275.20
7 8	290.00
8 homogenized B Ep	215.90

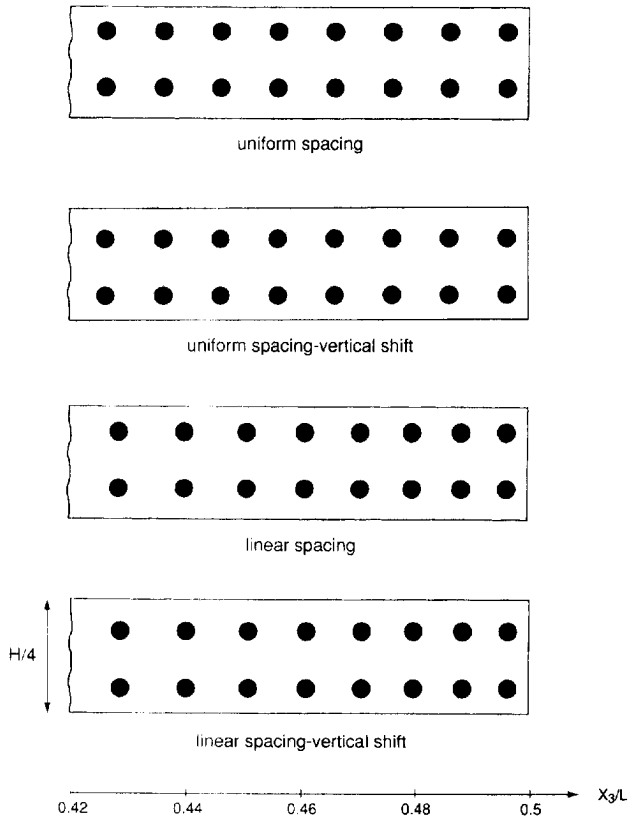

Fig. 13. Schematic of different fiber distributions in the B/Ep ply near the free edge.

uniformly shifting the two rows of fibers in the vertical direction while preserving the uniform horizontal fiber spacing. The third configuration was generated by linearly increasing the fiber spacing in the horizontal direction with increasing distance from the free edge, in the manner described previously, while preserving the vertical spacing of the baseline configuration. Finally, the fourth configuration was obtained from the third by vertically shifting the two rows of fibers in the same manner as was used to generate the second configuration. The total fibre volume fraction of the B/Ep region with the four fiber architectures considered was 0.50. The local fiber volume fractions of the vertical columns of cells in the uniformly spaced and linearly spaced fiber configurations are given in Table 4.

The resulting peel stress distributions along the B/Ep-Ti interface in the four configurations caused by the uniformly applied temperature change of $-154.45°C$ are illustrated in Fig. 14. Comparing the peel stress distribution in the uniformly spaced baseline configuration (Fig. 14a) with the stress distribution in the second configuration (Fig. 14b) we observe increased peel stress oscillations in the regions directly below the fiber locations.

Table 4. Local fiber volume fractions in the cells at the free edge

Cell number from free edge	v_f (uniform fiber spacing)	v_f (linearly increasing fiber spacing)
1	0.55	0.63
2	0.50	0.60
3	0.50	0.56
4	0.50	0.52
5	0.50	0.49
6	0.50	0.46
7	0.50	0.44
8	0.43	0.34

The fiber volume fraction in the 1st and 8th cells of the uniformly spaced configuration differs from 0.50 owing to horizontal shift of the fiber architecture towards the free edge as explained in the text.

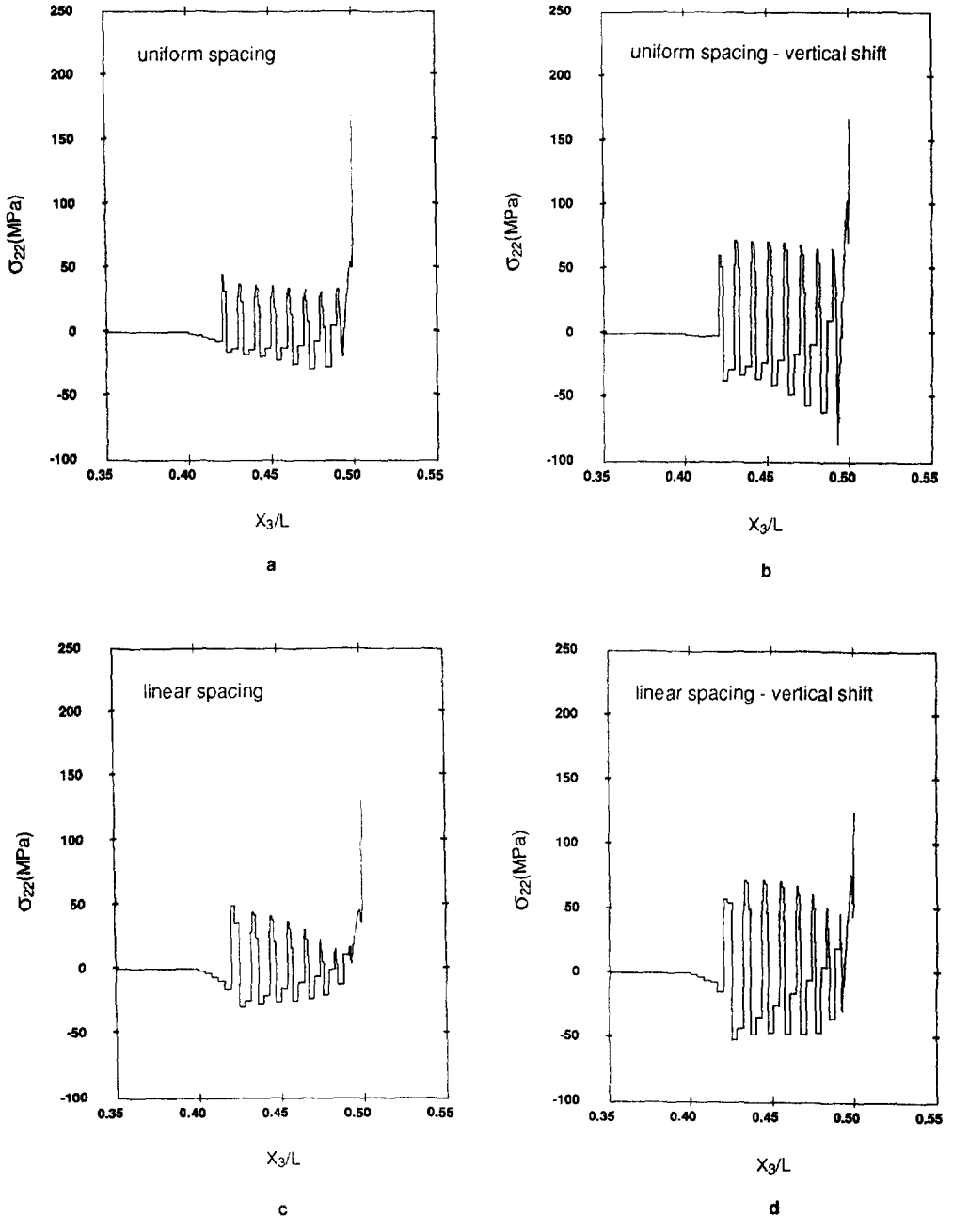

Fig. 14. Normal stress σ_{22} distributions in the titanium ply at the B Ep Ti interface near the free edge for the differently distributed fibers shown in Fig. 13.

The relative increase in the oscillations is caused by the reduced distance between the interface and the bottom row of fibers produced by the vertical shift. The vertical shift also produces a reduction in the maximum peel stress at the free edge relative to the baseline configuration. The peel stress distribution in the configuration with the linearly spaced fibers (Fig. 14c) exhibits decreasing oscillations with decreasing distance from the free edge relative to the baseline configuration. A substantially greater decrease in the maximum peel stress at the free edge relative to the baseline configuration is also observed, as compared to the free-edge peel stress reduction observed in the second configuration. Finally, the peel stress distribution in the fourth configuration presented in Fig. 14d exhibits characteristics that are peculiar to the second and third configuration. Here, we observe an increase in the peel stress oscillations relative to the baseline configuration that decrease with decreasing

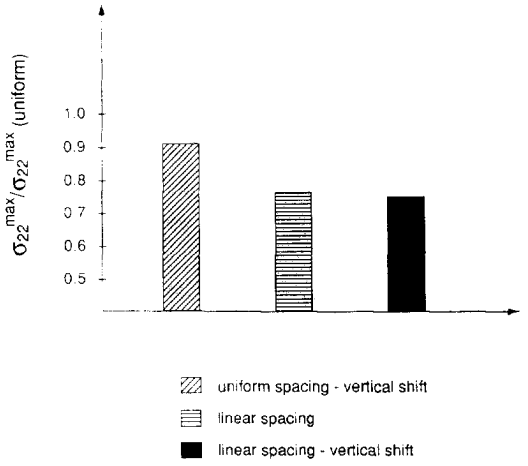

Fig. 15. Maximum stress σ_{22} in the titanium ply at the free-edge of the laminate at the interface separating B/Ep and Ti plies due to a temperature change of $\Delta T = -154.45$ C obtained from distributions of Fig. 14, normalized with respect to the corresponding maximum stress obtained from the configuration with uniformly spaced fibers.

distance from the free edge. The reduction in the maximum peel stress at the free edge also appears to be substantial, and slightly greater than in the third configuration. A more precise comparison of the maximum peel stress values at the free edge in the functionally graded configurations is presented in bar chart format in Fig. 15, normalized by the corresponding value of the uniformly spaced baseline configuration. As is observed, the greatest reduction in the peel stress (i.e. *ca* 25%) occurs when the fibers are both linearly spaced and vertically shifted. When the fibers are linearly spaced without the vertical shift, the reduction is approximately 24%, indicating that the additional vertical shift does not play a significant role in this case. In fact, the increased oscillations in the peel stress distribution caused by the vertical shift may not be desirable in some situations. Alternatively, when the fibers are vertically shifted without decreased horizontal spacing, the peel stress is reduced by a modest 9%. Thus it appears that the major contribution to the reduction of the free-edge peel stress comes from functional grading in the horizontal direction.

It is interesting to relate the reduction in the peel stress produced by the functional grading of fiber architecture to the reduction in the transverse thermal expansion mismatch between B/Ep and Ti plies with increasing fiber volume fraction illustrated in Fig. 4. As observed in the figure, the transverse thermal expansion mismatch decreases rapidly with increasing fiber volume content for fiber volume fractions greater than approximately 0.05. As observed in Table 4, the local fiber volume fractions in the first three vertical columns of cells in the uniformly spaced configurations are 0.55, 0.50 and 0.50, compared to 0.63, 0.60 and 0.56 in the linearly spaced configurations. Figure 4 indicates that the transverse thermal expansion coefficients in a B Ep ply with fiber volume fractions of 0.50, 0.55 and 0.63 are 32.50, 29.52 and 24.91 (10^{-6} C^{-1}), respectively. The relatively modest decrease in the local thermal expansion mismatch (approximately 14%) in the immediate vicinity of the free edge (i.e. the first three fibers) achieved by a correspondingly modest increase in the local fiber volume fraction (approximately 14%) thus produces a substantial reduction in the peel stress at the free edge (approximately 25%). This obviously has technologically significant implications.

4. SUMMARY AND CONCLUSIONS

A previously developed theory for the elastic response of metal matrix composites with a finite number of uniformly or nonuniformly spaced inclusions or fibers in the thickness

direction subjected to a through-thickness thermal gradient has been extended herein to enable analysis of material architectures characterized by nonuniform fiber spacing in two directions. In this new approach, the microstructural and macrostructural details are *explicitly coupled* when solving the thermomechanical boundary-value problem. Coupling of the local and global analyses allows one to rationally analyse the response of polymeric and metal matrix composites such as B/Ep, B/Al and SiC/TiAl that contain relatively few through-thickness fibers, as well as so-called functionally graded materials with continuously changing properties due to nonuniform fiber spacing or the presence of several phases. For this class of emerging composites, it is difficult, if not impossible, to define the representative volume element (RVE) used in the traditional micromechanical analyses of macroscopically homogeneous composites (Hill, 1963).

The extension of the theory to material architectures functionally graded in two directions makes possible the analysis of laminated composite plates with finite dimensions in one plane subjected to combined thermomechanical loading. In particular, the technologically important interlaminar stress fields in laminated composite plates in the vicinity of the free edge can be analysed with the outlined approach. The mismatch in the thermomechanical properties between adjacent plies in layered composites gives rise to severe stress concentrations at the free edge which often cause delamination failures. A review of the free-edge problem and a discussion of the associated failure modes in laminated composites has been given by Herakovich (1989).

The presented comparison of interlaminar stresses in a symmetrically laminated B/Ep-Ti plate subjected to a uniform temperature change generated using the new coupled approach and the finite-element method based on homogenized properties of the individual plies demonstrates the capability of the proposed theory to capture the large stress gradients at the free edge. Explicit incorporation of the microstructure of the B/Ep plies in the interlaminar stress calculations using the coupled theory produces maximum value for the peel stress at the free edge that is approximately 35% higher than the corresponding value based on the homogenized B/Ep ply properties (Fig. 10). This requires explicit consideration of at least seven columns of fibers localized at the free edge. Microstructures with fewer fibers produce stress fields that do not adequately reflect the actual stresses. Thus the calculation of the technologically important interlaminar peel stress at the free edge of a laminate based on the homogenized continuum approach substantially underestimates the actual stress fields, leading to unsafe designs.

In order to reduce the high interlaminar peel stress at the free edge, the local thermal expansion mismatch between the B/Ep and Ti plies must be reduced. This can be achieved by altering the microstructure of the B/Ep plies at the free edge through functional grading of the boron fiber distribution. By decreasing the fiber spacing with decreasing distance from the free edge the local fiber volume fraction in the B/Ep plies is increased, thus decreasing the transverse thermal expansion mismatch as observed in Fig. 4. Substantial reductions in the free-edge peel stress can be achieved by a relatively modest increase in the local fiber volume fraction directly at the free edge (see Fig. 15 and Table 4).

It should be emphasized that the new theory presented herein makes possible the investigation of the effects of fiber distribution and fiber shape in functionally graded composites. Recent investigation of these effects in doubly-periodic composites was conducted by Arnold *et al.* (1995) using the concept of a repeating unit cell. Such effects can now be investigated in the presence of a continuously changing microstructure in conjunction with the coupling of the micro and macro-structural response.

Finally, in previous investigations the authors have demonstrated that the inclusion of inelastic effects in the analysis of functionally graded materials may be important in the presence of large temperature gradients in applications involving one-dimensional version of the higher-order theory (cf. Pindera *et al.*, 1994; Aboudi *et al.*, 1995a). Others have demonstrated the importance of inelastic effects within the context of the free-edge problem. For example, Drake *et al.* (1993) and Williamson *et al.* (1993) employed the finite-element method to study the residual stresses that develop at graded ceramic-metal interfaces joining cylindrical bodies made of metallic and ceramic materials. The gradation was modeled using a series of perfectly bonded cylindrical layers, with each layer having slightly different

properties. Their results demonstrate the importance of plasticity effects in the analysis of graded and non-graded interfaces. The authors also showed that in some cases optimization of the microstructure of graded layers is required to achieve reduction in certain critical stress components that control interfacial failure. Along similar lines, Suresh *et al.* (1994) studied the response of elastoplastic bimaterial strips subjected to cyclic temperature variations. Closed-form solutions were derived using simple beam and plate theories to analyse the stresses and curvature that develop in a bimaterial configuration for the considered thermal loading. In addition, finite-element formulation was employed to capture other features not included in the simple analytical models. In particular, the authors showed that the plastic flow along the interface separating the two materials at the free edge can be modified substantially by altering the constraints at the edges of the strip. Therefore, in subsequent investigations inelasticity effects will be incorporated into the theoretical framework of HOTFGM-2D.

Acknowledgements—The first two authors gratefully acknowledge the support provided by the NASA-Lewis Research Center through the grant NASA NAG 3-1377. The authors are grateful to Professor Furman W. Barton, Chair of the Civil Engineering and Applied Mechanics Department at the University of Virginia for providing partial support during the first author's sabbatical leave. Fruitful discussions with Professor Carl T. Herakovich about the thermal free-edge problem are also much appreciated.

REFERENCES

Aboudi, J. (1991). *Mechanics of Composite Materials—A Unified Micromechanical Approach*. Elsevier, New York.

Aboudi, J., Pindera, M.-J. and Arnold, S. M. (1993). Thermoelastic response of large-diameter fiber metal matrix composites to thermal gradients. NASA TM 106344. NASA-Lewis Research Center, Cleveland, OH.

Aboudi, J., Arnold, S. M. and Pindera, M.-J. (1994a). Response of functionally graded composites to thermal gradients. *Compos. Engng* **4,** 1–18.

Aboudi, J., Pindera, M.-J. and Arnold, S. M. (1994b). Elastic response of metal matrix composites with tailored microstructures to thermal gradients. *Int. J. Solids Structures* **31,** 1393–1428.

Aboudi, J., Pindera, M.-J. and Arnold, S. M. (1995a). Thermo-inelastic response of functionally graded composites. *Int. J. Solids Structures* **32,** 1675–1710.

Aboudi, J., Pindera, M.-J. and Arnold, S. M. (1995b). A coupled higher-order theory for functionally graded composites with partial homogenization. *Compos. Engng* (In press).

Arnold, S. M., Pindera, M.-J. and Wilt, T. E. (1995). Influence of the fiber architecture on the elastic and inelastic response of metal matrix composites. NASA TM 106705. NASA-Lewis Research Center, Cleveland, OH.

Drake, J. T., Williamson, R. L. and Rabin, B. H. (1993). Finite element analysis of thermal residual stresses at graded ceramic–metal interfaces. Part II. Interface optimization for residual stress reduction. *J. Appl. Phys.* **74,** 1321–1326.

Fukushima, T. (ed.) (1992). *Proceedings of the International Workshop on Functionally Gradient Composites*, 5–6 November 1992. Hilton Square, San Francisco, USA. Japan International Science and Technology Exchange Center.

Herakovich, C. T. (1976). On thermal edge effects in composite laminates. *Int. J. Mech. Sci.* **18,** 129–134.

Herakovich, C. T. (1989). Free edge effects in laminated composites. In *Handbook of Composites*, Vol. 2 *Structures and Design* (eds C. T. Herakovich and Y. M. Tarnopol'skii). Elsevier, Amsterdam.

Hill, R. (1963). Elastic properties of reinforced solids: some theoretical principles. *J. Mech. Phys. Solids* **11,** 357–372.

Malvern, L. E. (1969). *Introduction to the Mechanics of a Continuous Medium*. Prentice-Hall, Englewood Cliffs, New Jersey.

Pindera, M.-J. and Dunn, P. (1995). An evaluation of a coupled microstructural approach for the analysis of functionally graded composites via finite-element method. NASA CR 195455. NASA-Lewis Research Center, Cleveland, OH.

Pindera, M.-J., Aboudi, J. and Arnold, S. M. (1994). Thermo-inelastic analysis of functionally graded materials: inapplicability of the classical micromechanics approach. In *Inelasticity and Micromechanics of Metal Matrix Composites* (eds G. Z. Voyiadjis and J. W. Ju), pp. 273–305. Elsevier, Amsterdam.

Pindera, M.-J., Aboudi, J. and Arnold, S. M. (1995). Limitations of the uncoupled, RVE-based micromechanical approach in the analysis of functionally graded composites. *Mech. Mater.* **20,** 77–94.

Suresh, S., Giannakopoulos, A. E. and Olsson, M. (1994). Elastoplastic analysis of thermal cycling: layered materials with sharp interfaces. *J. Mech. Phys. Solids* **42,** 979–1018.

Wakashima, K. and Tsukamoto, H. (1990). Micromechanical approach to the thermomechanics of ceramic–metal gradient materials. *Proceedings First Int. Symposium on Functionally Gradient Materials*, pp. 19–26, Sendai, Japan.

Williamson, R. L., Rabin, B. H. and Drake, J. T. (1993). Finite element analysis of thermal residual stresses at graded ceramic–metal interfaces. Part I. Model description and geometrical effects. *J. Appl. Phys.* **74,** 1310–1320.

APPENDIX A: THERMAL ANALYSIS

Heat conduction equations

Multiplying eqn (1) by $(\bar{x}_1^{(\alpha)})^l (\bar{x}_2^{(\beta)})^m (\bar{x}_3^{(\gamma)})^n$, where $l, m, n = 0, 1$, or 2 with $l+m+n \leqslant 2$, and integrating by parts, using the temperature expansion given in eqn (9), the following equations are obtained:

$$L^{(\alpha\beta\gamma)}_{1(0,0,0)} + L^{(\alpha\beta\gamma)}_{2(0,0,0)} + L^{(\alpha\beta\gamma)}_{3(0,0,0)} = 0 \tag{A1}$$

$$L^{(\alpha\beta\gamma)}_{2(0,1,0)} - Q^{(\alpha\beta\gamma)}_{2(0,0,0)} = 0 \tag{A2}$$

$$L^{(\alpha\beta\gamma)}_{3(0,0,1)} - Q^{(\alpha\beta\gamma)}_{3(0,0,0)} = 0 \tag{A3}$$

$$\tfrac{1}{12}d_2^2[3L^{(\alpha\beta\gamma)}_{1(0,0,0)} + L^{(\alpha\beta\gamma)}_{2(0,0,0)} + L^{(\alpha\beta\gamma)}_{3(0,0,0)}] - 2Q^{(\alpha\beta\gamma)}_{1(0,0,0)} = 0 \tag{A4}$$

$$\tfrac{1}{12}h_\beta^{(q)2}[L^{(\alpha\beta\gamma)}_{1(0,0,0)} + 3L^{(\alpha\beta\gamma)}_{2(0,0,0)} + L^{(\alpha\beta\gamma)}_{3(0,0,0)}] - 2Q^{(\alpha\beta\gamma)}_{2(0,1,0)} = 0 \tag{A5}$$

$$\tfrac{1}{12}l^{(r)2}[L^{(\alpha\beta\gamma)}_{1(0,0,0)} + L^{(\alpha\beta\gamma)}_{2(0,0,0)} + 3L^{(\alpha\beta\gamma)}_{3(0,0,0)}] - 2Q^{(\alpha\beta\gamma)}_{3(0,0,1)} = 0, \tag{A6}$$

where $Q^{(\alpha\beta\gamma)}_{n(l,m,n)}$ has been defined previously in eqn (10), and

$$L^{(\alpha\beta\gamma)}_{1(0,0,0)} = \frac{1}{v^{(pqr)}_{(\alpha\beta\gamma)}} \int_{-h_\beta^{(q)}/2}^{h_\beta^{(q)}/2} \int_{-l^{(r)}/2}^{l^{(r)}/2} \left[q_1^{(\alpha\beta\gamma)}\left(\frac{d_\alpha}{2}\right) - q_1^{(\alpha\beta\gamma)}\left(-\frac{d_\alpha}{2}\right)\right] \mathrm{d}\bar{x}_2^{(\beta)}\,\mathrm{d}\bar{x}_3^{(\gamma)} \tag{A7}$$

$$L^{(\alpha\beta\gamma)}_{2(0,n,0)} = \frac{1}{v^{(pqr)}_{(\alpha\beta\gamma)}} \left(\frac{h_\beta^{(q)}}{2}\right)^n \int_{-d_\alpha/2}^{d_\alpha/2} \int_{-l^{(r)}/2}^{l^{(r)}/2} \left[q_2^{(\alpha\beta\gamma)}\left(\frac{h_\beta^{(q)}}{2}\right) + (-1)^n q_2^{(\alpha\beta\gamma)}\left(-\frac{h_\beta^{(q)}}{2}\right)\right] \mathrm{d}\bar{x}_1^{(\alpha)}\,\mathrm{d}\bar{x}_3^{(\gamma)} \tag{A8}$$

$$L^{(\alpha\beta\gamma)}_{3(0,0,n)} = \frac{1}{v^{(pqr)}_{(\alpha\beta\gamma)}} \left(\frac{l^{(r)}}{2}\right)^n \int_{-d_\alpha/2}^{d_\alpha/2} \int_{-h_\beta^{(q)}/2}^{h_\beta^{(q)}/2} \left[q_3^{(\alpha\beta\gamma)}\left(\frac{l^{(r)}}{2}\right) + (-1)^n q_3^{(\alpha\beta\gamma)}\left(-\frac{l^{(r)}}{2}\right)\right] \mathrm{d}\bar{x}_1^{(\alpha)}\,\mathrm{d}\bar{x}_2^{(\beta)}. \tag{A9}$$

In the above: $n = 0$ or 1; $q_1^{(\alpha\beta\gamma)}(\pm d_\alpha/2)$, $q_2^{(\alpha\beta\gamma)}(\pm h_\beta^{(q)}/2)$, $q_3^{(\alpha\beta\gamma)}(\pm l^{(r)}/2)$ denote the interfacial fluxes at $\bar{x}_1^{(\alpha)} = \pm\frac{1}{2}d_\alpha$, $\bar{x}_2^{(\beta)} = \pm\frac{1}{2}h_\beta^{(q)}$, $\bar{x}_3^{(\gamma)} = \pm\frac{1}{2}l^{(r)}$, respectively; and $v^{(pqr)}_{(\alpha\beta\gamma)} = d_\alpha h_\beta^{(q)} l^{(r)}$ is the volume of the subcell $(\alpha\beta\gamma)$ in the (p,q,r)th cell.

Equations (A1)–(A6) provide relations between the zeroth-order and first order heat fluxes $Q^{(\alpha\beta\gamma)}_{n(l,m,n)}$ and the interfacial fluxes $L^{(\alpha\beta\gamma)}_{n(l,m,n)}$. Explicit expressions for the interfacial fluxes $L^{(\alpha\beta\gamma)}_{n(l,m,n)}$ given solely in terms of $Q^{(\alpha\beta\gamma)}_{n(l,m,n)}$ are obtained through the following sequence of manipulations, noting that eqns (A2) and (A3) already provide direct relations between $Q^{(\alpha\beta\gamma)}_{2(0,0,0)}$ and $L^{(\alpha\beta\gamma)}_{2(0,1,0)}$, and $Q^{(\alpha\beta\gamma)}_{3(0,0,0)}$ and $L^{(\alpha\beta\gamma)}_{3(0,0,1)}$. First, substituting eqn (A1) into (A5) and (A6), respectively, gives the following direct expressions for $L^{(\alpha\beta\gamma)}_{2(0,0,0)}$ and $L^{(\alpha\beta\gamma)}_{3(0,0,0)}$.

$$L^{(\alpha\beta\gamma)}_{2(0,0,0)} = 12Q^{(\alpha\beta\gamma)}_{2(0,1,0)}/h_\beta^{(q)2} \tag{A10}$$

$$L^{(\alpha\beta\gamma)}_{3(0,0,0)} = 12Q^{(\alpha\beta\gamma)}_{3(0,0,1)}/l^{(r)2}. \tag{A11}$$

Then upon substitution of eqns (A10) and (A11) into (A1) we obtain the following expression for $L^{(\alpha\beta\gamma)}_{1(0,0,0)}$.

$$L^{(\alpha\beta\gamma)}_{1(0,0,0)} = -12(Q^{(\alpha\beta\gamma)}_{2(0,1,0)}/h_\beta^{(q)2} + Q^{(\alpha\beta\gamma)}_{3(0,0,1)}/l^{(r)2}) \tag{A12}$$

Equations (A10) to (A12) will be used to reduce the heat conduction and heat flux continuity equations to expressions involving only the heat flux quantities $Q^{(\alpha\beta\gamma)}_{n(l,m,n)}$. These can subsequently be expressed in terms of the fundamental unknown coefficients $T^{(\alpha\beta\gamma)}_{(lmn)}$ appearing in the temperature expansion given by eqns (9), using eqns (11)–(15).

Heat flux continuity equations

The heat flux continuity conditions (3)–(4) are imposed on an average basis at each subcell and cell interface. The heat flux condition in the x_1 direction is obtained using eqn (3a) in (A7), yielding

$$[d_1 L^{(\alpha\beta\gamma)}_{1(000)} + d_2 L^{(\alpha\beta\gamma)}_{1(010)}]^{(pqr)}_{(\alpha\beta\gamma)} = 0. \tag{A13}$$

We note that eqn (4a) is identically satisfied for a material that is periodic in the x_1 direction by the chosen temperature field representation.

Prior to imposing the continuity conditions in the FG x_2 and x_3 directions, let us define intermediate quantities $f_l^{(\alpha\beta\gamma)}$ and $g_l^{(\alpha\beta\gamma)}$ as follows:

$$f_2^{(\alpha\beta\gamma)}|^{(pqr)} = q_2^{(\alpha\beta\gamma)}|^{(pqr)}_{y^{(pqr)}_{(\alpha\beta\gamma)}=h_\beta^{(q)}/2} - q_2^{(\alpha\beta\gamma)}|^{(pqr)}_{y^{(pqr)}_{(\alpha\beta\gamma)}=-h_\beta^{(q)}/2} \tag{A14}$$

$$g_2^{(\alpha\beta\gamma)}|^{(pqr)} = q_2^{(\alpha\beta\gamma)}|^{(pqr)}_{y^{(pqr)}_{(\alpha\beta\gamma)}=h_\beta^{(q)}/2} + q_2^{(\alpha\beta\gamma)}|^{(pqr)}_{y^{(pqr)}_{(\alpha\beta\gamma)}=-h_\beta^{(q)}/2} \tag{A15}$$

These quantities will simplify the algebra associated with application of the heat flux continuity requirement on an average basis in the x_2 FG direction. Then substituting eqns (3b) and (4b) into the above definitions, we have

$$f_2^{(\alpha 1;\gamma)}|^{(p,q,r)} = q_2^{(\alpha 2;\gamma)}|^{(p,q,r)}_{\bar{x}_2^{(\gamma)} = -h_2^{(q)}/2} - q_2^{(\alpha 2;\gamma)}|^{(p,q-1,r)}_{\bar{x}_2^{(\gamma)} = h_2^{(q-1)}/2} \tag{A16}$$

$$g_2^{(\alpha 1;\gamma)}|^{(p,q,r)} = q_2^{(\alpha 2;\gamma)}|^{(p,q,r)}_{\bar{x}_2^{(\gamma)} = -h_2^{(q)}/2} + q_2^{(\alpha 2;\gamma)}|^{(p,q-1,r)}_{\bar{x}_2^{(\gamma)} = h_2^{(q-1)}/2}. \tag{A17}$$

Adding and subtracting equal quantities to and from eqns (A16) and (A17) it can easily be verified that

$$2f_2^{(\alpha 1;\gamma)}|^{(p,q,r)} = [-f_2^{(\alpha 2;\gamma)} + g_2^{(\alpha 2;\gamma)}]^{(p,q,r)} - [f_2^{(\alpha 2;\gamma)} + g_2^{(\alpha 2;\gamma)}]^{(p,q-1,r)} \tag{A18}$$

$$2g_2^{(\alpha 1;\gamma)}|^{(p,q,r)} = [-f_2^{(\alpha 2;\gamma)} + g_2^{(\alpha 2;\gamma)}]^{(p,q,r)} + [f_2^{(\alpha 2;\gamma)} + g_2^{(\alpha 2;\gamma)}]^{(p,q-1,r)}. \tag{A19}$$

Then using eqns (A18) and (A19) in (A8), we obtain the following heat flux continuity conditions for the x_2 FG direction:

$$\left[-h_1 L^{(\alpha 1;\gamma)}_{2(0,0,0)} + L^{(\alpha 2;\gamma)}_{2(0,1,0)} - \frac{h_2}{2} L^{(\alpha 2;\gamma)}_{2(0,0,0)}\right]^{(p,q,r)} - \left[L^{(\alpha 2;\gamma)}_{2(0,1,0)} + \frac{h_2}{2} L^{(\alpha 2;\gamma)}_{2(0,0,0)}\right]^{(p,q-1,r)} = 0 \tag{A20}$$

$$\left[-L^{(\alpha 1;\gamma)}_{2(0,1,0)} + \frac{1}{2} L^{(\alpha 2;\gamma)}_{2(0,1,0)} - \frac{h_2}{4} L^{(\alpha 2;\gamma)}_{2(0,0,0)}\right]^{(p,q,r)} + \frac{1}{2}\left[L^{(\alpha 2;\gamma)}_{2(0,1,0)} + \frac{h_2}{2} L^{(\alpha 2;\gamma)}_{2(0,0,0)}\right]^{(p,q-1,r)} = 0. \tag{A21}$$

Similarly, the heat flux continuity conditions (3c) and (4c) in the remaining x_3 FG direction provide

$$\left[-l_1 L^{(\alpha\beta 1)}_{3(0,0,0)} + L^{(\alpha\beta 2)}_{3(0,0,1)} - \frac{l_2}{2} L^{(\alpha\beta 2)}_{3(0,0,0)}\right]^{(p,q,r)} - \left[L^{(\alpha\beta 2)}_{3(0,0,1)} + \frac{l_2}{2} L^{(\alpha\beta 2)}_{3(0,0,0)}\right]^{(p,q,r-1)} = 0 \tag{A22}$$

and

$$\left[-L^{(\alpha\beta 1)}_{3(0,0,1)} + \frac{1}{2} L^{(\alpha\beta 2)}_{3(0,0,1)} - \frac{l_2}{4} L^{(\alpha\beta 2)}_{3(0,0,0)}\right]^{(p,q,r)} + \frac{1}{2}\left[L^{(\alpha\beta 2)}_{3(0,0,1)} + \frac{l_2}{2} L^{(\alpha\beta 2)}_{3(0,0,0)}\right]^{(p,q,r-1)} = 0. \tag{A23}$$

Equations (A10)–(A12), together with eqns (A2) and (A3), will be employed in reducing the heat flux continuity conditions (A13), (A20)–(A23) to expressions involving only the volume-averaged zeroth-order and first-order heat flux quantities $Q^{(\alpha\beta;\gamma)}_{i(l,m,n)}$.

Reduction of heat conduction and heat flux continuity equations

Substituting eqn (A1) into (A4), and using eqns (A10) and (A11), reduces the volume-averaged heat conduction equations to a set of eight equations given by eqn (16). Next, using the expression for $L^{(\alpha\beta;\gamma)}_{1(0,0,0)}$ given by eqn (A12), and the expression for $L^{(\alpha\beta;\gamma)}_{2(0,1,0)}$ given by eqn (A2), and $L^{(\alpha\beta;\gamma)}_{3(0,0,1)}$ given by eqn (A3), in the continuity relations (A13), (A20)–(A23), we obtain eqns (17) and (21).

Thermal continuity equations

As in the case of the heat flux field, the thermal continuity conditions (5)–(6) are imposed on an average basis at each subcell and cell interface. Thus substituting eqn (9) into eqns (5a–c), respectively, we obtain at each subcell interface the conditions (22), (23) and (25). Furthermore, substituting eqn (9) into eqns (6b–c) to ensure continuity of temperature between neighboring cells in the FG directions, we obtain the conditions (24) and (26).

APPENDIX B: MECHANICAL ANALYSIS

Equations of equilibrium

Let us multiply eqn (28) by $(\bar{x}_1^{(\alpha)})^l (\bar{x}_2^{(\beta)})^m (\bar{x}_3^{(\gamma)})^n$, where again $l, m, n, = 0, 1$, or 2 with $l+m+n \leqslant 2$. Integrating the resulting equations by parts, and using the displacement expansions (37), we obtain the equations of equilibrium in the subcell region $(\alpha\beta\gamma)$ in the form:

$$I^{(\alpha\beta;\gamma)}_{1(0,0,0)} + J^{(\alpha\beta;\gamma)}_{2(0,0,0)} + K^{(\alpha\beta;\gamma)}_{3(0,0,0)} = 0 \tag{B1}$$

$$I^{(\alpha\beta;\gamma)}_{1(1,0,0)} = S^{(\alpha\beta;\gamma)}_{1(0,0,0)} \tag{B2}$$

$$J^{(\alpha\beta;\gamma)}_{2(0,1,0)} = S^{(\alpha\beta;\gamma)}_{2(0,0,0)} \tag{B3}$$

$$K^{(\alpha\beta;\gamma)}_{3(0,0,1)} = S^{(\alpha\beta;\gamma)}_{3(0,0,0)} \tag{B4}$$

$$\frac{1}{12} d_\alpha^2 [3I^{(\alpha\beta;\gamma)}_{1(0,0,0)} + J^{(\alpha\beta;\gamma)}_{2(0,0,0)} + K^{(\alpha\beta;\gamma)}_{3(0,0,0)}] - 2S^{(\alpha\beta;\gamma)}_{1(1,0,0)} = 0 \tag{B5}$$

$$\frac{1}{12} h_\beta^{(q)2} [I^{(\alpha\beta;\gamma)}_{1(0,0,0)} + 3J^{(\alpha\beta;\gamma)}_{2(0,0,0)} + K^{(\alpha\beta;\gamma)}_{3(0,0,0)}] - 2S^{(\alpha\beta;\gamma)}_{2(0,1,0)} = 0 \tag{B6}$$

$$\frac{1}{12} l^{(\gamma)2} [I^{(\alpha\beta;\gamma)}_{1(0,0,0)} + J^{(\alpha\beta;\gamma)}_{2(0,0,0)} + 3K^{(\alpha\beta;\gamma)}_{3(0,0,0)}] - 2S^{(\alpha\beta;\gamma)}_{3(0,0,1)} = 0, \tag{B7}$$

where $j = 2,3$ in eqns (B1) and (B3)–(B7), while in equation (B2) $j = 1$. In the above equations, $S^{(\alpha\beta;)}_{ij(lm,n)}$ has been defined previously in eqn (38), and

$$I^{(\alpha\beta;)}_{1;(a,0,0)} = \frac{1}{V_{(\alpha\beta)}}(\tfrac{1}{2}d_2)^{a}\int_{\cdot}^{\cdot}\int_{\cdot}^{\cdot}[\sigma_1^{(\alpha\beta;)}(\tfrac{1}{2}d_2)+(-1)^{a+1}\sigma_1^{(\alpha\beta;)}(-\tfrac{1}{2}d_2)]\,\mathrm{d}\bar{x}_2^{(\beta)}\,\mathrm{d}\bar{x}_3^{(\gamma)} \tag{B8}$$

$$J^{(\alpha\beta;)}_{2;(0,n,0)} = \frac{1}{V_{(\alpha\beta;)}}(\tfrac{1}{2}h_\beta^{(\alpha)})^{n}\int_{\cdot}^{\cdot}\int_{\cdot}^{\cdot}[\sigma_2^{(\alpha\beta;)}(\tfrac{1}{2}h_\beta^{(\alpha)})+(-1)^{n+1}\sigma_2^{(\alpha\beta;)}(-\tfrac{1}{2}h_\beta^{(\alpha)})]\,\mathrm{d}\bar{x}_1^{(\alpha)}\,\mathrm{d}\bar{x}_3^{(\gamma)} \tag{B9}$$

$$K^{(\alpha\beta;)}_{3;(0,0,n)} = \frac{1}{V_{(\alpha\beta;)}}(\tfrac{1}{2}l^{(\gamma)})^{n}\int_{\cdot}^{\cdot}\int_{\cdot}^{\cdot}[\sigma_3^{(\alpha\beta;)}(\tfrac{1}{2}l^{(\gamma)})+(-1)^{n+1}\sigma_3^{(\alpha\beta;)}(-\tfrac{1}{2}l^{(\gamma)})]\,\mathrm{d}\bar{x}_1^{(\alpha)}\,\mathrm{d}\bar{x}_2^{(\beta)}. \tag{B10}$$

In the above: $n = 0$ or 1; $\sigma_1^{(\alpha\beta;)}(\pm\frac{1}{2}d_2)$, $\sigma_2^{(\alpha\beta;)}(\pm\frac{1}{2}h_\beta^{(\alpha)})$, $\sigma_3^{(\alpha\beta;)}(\pm\frac{1}{2}l^{(\gamma)})$, stand for the interfacial stresses at $\bar{x}_1^{(\alpha)} = \pm\frac{1}{2}d_2, \bar{x}_2^{(\beta)} = \pm\frac{1}{2}h_\beta^{(\alpha)}, \bar{x}_3^{(\gamma)} = \pm\frac{1}{2}l^{(\gamma)}$, respectively.

Equations (B1)–(B7) provide relations between the zeroth-order and first order, volume-averaged stresses $S^{(\alpha\beta;)}_{ij(lm,n)}$ and the interfacial tractions $I^{(\alpha\beta;)}_{1;(n,0,0)}$, $J^{(\alpha\beta;)}_{2;(0,n,0)}$ and $K^{(\alpha\beta;)}_{3;(0,0,n)}$. Direct "one-to-one" relations are obtained through the following sequence of manipulations, noting that eqns (B2)–(B4) already provide direct relations between $S^{(\alpha\beta;)}_{11(0,0,0)}$ and $I^{(\alpha\beta;)}_{111(1,0,0)}$, $S^{(\alpha\beta;)}_{2j(0,0,0)}$ and $J^{(\alpha\beta;)}_{2j(0,1,0)}$, $S^{(\alpha\beta;)}_{3j(0,0,0)}$ and $K^{(\alpha\beta;)}_{3j(0,0,1)}$, $j = 2, 3$. First, substituting eqn (B1) into eqns (B6) and (B7), respectively, gives direct expressions for $J^{(\alpha\beta;)}_{2;(0,0,0)}$ and $K^{(\alpha\beta;)}_{3;(0,0,0)}$:

$$J^{(\alpha\beta;)}_{2;(0,0,0)} = 12S^{(\alpha\beta;)}_{2j(0,1,0)}h^{(\alpha)}_{\beta} \tag{B11}$$

$$K^{(\alpha\beta;)}_{3;(0,0,0)} = 12S^{(\alpha\beta;)}_{3j(0,0,1)}l^{(\gamma)}. \tag{B12}$$

Then, upon substitution of eqns (B11) and (B12) into (B1), we have the following expression for $I^{(\alpha\beta;)}_{1;(0,0,0)}$:

$$I^{(\alpha\beta;)}_{1;(0,0,0)} = -12(S^{(\alpha\beta;)}_{2j(0,1,0)}h^{(\alpha)}_{\beta} + S^{(\alpha\beta;)}_{3j(0,0,1)}l^{(\gamma)}). \tag{B13}$$

Equations (B11)–(B13) will be used to reduce the equilibrium equations and traction continuity equations to expressions involving only the zeroth-order and first-order, volume-averaged stress quantities $S^{(\alpha\beta;)}_{ij(lm,n)}$. These can subsequently be expressed in terms of the fundamental unknown coefficients $W^{(\alpha\beta;)}_{nlmn}$ appearing in the displacement field expansion given by eqns (37), using eqns (39)–(46).

Traction continuity conditions

The traction continuity conditions, eqns (31)–(32), are imposed on an average basis at the subcell and cell interfaces. These conditions imply existence of certain relationships between the surface integrals of the interfacial traction components defined by eqns (B8)–(B10). The normal traction continuity condition in the x_1 periodic direction is obtained using eqn (31a) in (B8) with $j = 1$. This yields

$$[I^{(\alpha\beta;)}_{1;(0,0,0)} - I^{(\alpha'\beta';)}_{1;(0,0,0)}]^{(\gamma\gamma')} = 0 \tag{B14}$$

We note that eqn (32a) is identically satisfied for $j = 1$.

For the shear traction continuity conditions in the x_2 direction we obtain from eqn (31a) and (B8) with $j = 2,3$

$$[d_1I^{(\alpha\beta;)}_{2;(0,0,0)} + d_2I^{(\alpha\beta;)}_{1;(0,0,0)}]^{(\gamma\gamma')} = 0 \tag{B15}$$

Again, eqn (32a) is identically satisfied for $j = 2,3$.

To assist in establishing the continuity relations in the FG directions, let us define two new quantities $F^{(\alpha\beta;)}_{\eta}$ and $G^{(\alpha\beta;)}_{\eta}$ as follows

$$F^{(\alpha\beta;)}_{\eta} = \sigma_2^{(\alpha\beta;)}[\eta, \tfrac{1}{2}h^{(\alpha)}_{\beta}] - \sigma_2^{(\alpha\beta;)}[\eta, -\tfrac{1}{2}h^{(\alpha)}_{\beta}] \tag{B16}$$

$$G^{(\alpha\beta;)}_{\eta} = \sigma_3^{(\alpha\beta;)}[\eta, \tfrac{1}{2}l^{(\gamma)}] + \sigma_3^{(\alpha\beta;)}[\eta, -\tfrac{1}{2}l^{(\gamma)}] \tag{B17}$$

Substituting eqns (31b) and (32b) into the above definitions, we obtain, respectively:

$$F^{(\alpha\beta;)}_{\eta} = \sigma_2^{(\alpha\beta;)}[\eta, \tfrac{1}{2}h^{(\alpha)}_{\beta}] - \sigma_2^{(\alpha'\beta';)}[\eta, -\tfrac{1}{2}h^{(\alpha')}_{\beta'}] \tag{B18}$$

$$G^{(\alpha\beta;)}_{\eta} = \sigma_3^{(\alpha\beta;)}[\eta, \tfrac{1}{2}l^{(\gamma)}] + \sigma_3^{(\alpha'\beta';)}[\eta, -\tfrac{1}{2}l^{(\gamma')}] \tag{B19}$$

By addition and subtraction of equal quantities to and from eqns (B18) and (B19) it can easily be verified that

$$2F^{(\alpha\beta;)}_{\eta} = [F^{(\alpha\beta;)}_{\eta} + G^{(\alpha\beta;)}_{\eta}] - [F^{(\alpha'\beta';)}_{\eta} + G^{(\alpha'\beta';)}_{\eta}] \tag{B20}$$

$$2G^{(\alpha\beta;)}_{\eta} = [G^{(\alpha\beta;)}_{\eta} - F^{(\alpha\beta;)}_{\eta}] + [G^{(\alpha'\beta';)}_{\eta} + F^{(\alpha'\beta';)}_{\eta}]. \tag{B21}$$

Then employing eqns (B20) and (B21) in eqn (B9) with $j = 2,3$ we obtain the corresponding relations:

$$[-h_1 J^{(\alpha 1;1)}_{2j(0,0,0)} + J^{(\alpha 2;1)}_{2j(0,1,0)} - \tfrac{1}{2}h_2 J^{(\alpha 2;1)}_{2j(0,0,0)}]^{(p,q,r)} - [J^{(\alpha 2;1)}_{2j(0,1,0)} + \tfrac{1}{2}h_2 J^{(\alpha 2;1)}_{2j(0,0,0)}]^{(p,q-1,r)} = 0 \tag{B22}$$

$$[-J^{(\alpha 1;1)}_{2j(0,1,0)} + \tfrac{1}{2}J^{(\alpha 2;1)}_{2j(0,1,0)} - \tfrac{1}{4}h_2 J^{(\alpha 2;1)}_{2j(0,0,0)}]^{(p,q,r)} + \tfrac{1}{2}[J^{(\alpha 2;1)}_{2j(0,1,0)} + \tfrac{1}{2}h_2 J^{(\alpha 2;1)}_{2j(0,0,0)}]^{(p,q-1,r)} = 0. \tag{B23}$$

Similarly, using eqns (31c) and (32c) with $j = 2,3$ we have

$$[-l_1 K^{(\alpha\beta 1)}_{3j(0,0,0)} + K^{(\alpha\beta 2)}_{3j(0,0,1)} - \tfrac{1}{2}l_2 K^{(\alpha\beta 2)}_{3j(0,0,0)}]^{(p,q,r)} - [K^{(\alpha\beta 2)}_{3j(0,0,1)} + \tfrac{1}{2}l_2 K^{(\alpha\beta 2)}_{3j(0,0,0)}]^{(p,q,r-1)} = 0 \tag{B24}$$

$$[-K^{(\alpha\beta 1)}_{3j(0,0,1)} + \tfrac{1}{2}K^{(\alpha\beta 2)}_{3j(0,0,1)} - \tfrac{1}{4}l_2 K^{(\alpha\beta 2)}_{3j(0,0,0)}]^{(p,q,r)} + \tfrac{1}{2}[K^{(\alpha\beta 2)}_{3j(0,0,1)} + \tfrac{1}{2}l_2 K^{(\alpha\beta 2)}_{3j(0,0,0)}]^{(p,q,r-1)} = 0. \tag{B25}$$

As a result of the above manipulations, 44 relations, given by eqns (B14)–(B15) and (B22)–(B25), arise from the traction continuity conditions between subcells and between neighboring cells. These equations, in conjunction with eqns (B2)–(B4) and (B11)–(B13), will be employed in reducing the equilibrium and traction continuity equations to expressions involving only volume-averaged zeroth-order and first-order stresses $S^{(\alpha\beta;r)}_{ij(l,m,n)}$.

Reduction of equilibrium and traction continuity equations

Substituting eqn (B1) into eqn (B5) and using eqns (B11) and (B12) reduces the volume-averaged equilibrium equations to a set of 16 equations given by eqn (47). Next, combining the expressions for $I^{(\alpha\beta;r)}_{11(1,0,0)}$ and $I^{(\alpha\beta;r)}_{11(0,0,0)}$, provided by eqns (B2) and (B13), and the continuity relations (B14)–(B15), respectively, we obtain the 12 equations given by (48)–(50). Continuing, if we substitute eqn (B3) and (B11) into eqns (B22)–(B23) directly, we obtain eqns (51) and (52), respectively. Finally, combining equations (B4) and (B12), and eqns (B24) and (B25), yields eqns (53) and (54), respectively.

Displacement continuity conditions

The displacement continuity conditions, i.e. eqns (33)–(34), are now imposed on an average basis at the interfaces. This is accomplished by first substituting eqn (37) into eqn (33a), yielding eqns (55)–(57), then into eqns (33b)–(34b), yielding eqns (58)–(61), followed by eqns (33c)–(34c), yielding eqns (62) and (65). Consequently, eqns (55)–(65) provide 44 relations which must be imposed to guarantee the continuity of the displacements between the subcells and between neighboring cells.